p53 isoforms have a high aggregation propensity, interact with chaperones and lack binding to p53 interaction partners

Anamari Brdar[1*], Christian Osterburg[1*#], Philipp Münick[1*], Anne Christin Machel[1], Rajeshwari Rathore[2], Susanne Osterburg[1], Büşra Yüksel[1,3], Birgit Schäfer[1], Kristina Desch[4,5], Julian D. Langer[5], Ivan Dikic[2,6,7] and Volker Dötsch[1#]

[1]Institute of Biophysical Chemistry and Center for Biomolecular Magnetic Resonance, Goethe University, 60438 Frankfurt, Germany.

[2]Institute of Biochemistry II, Faculty of Medicine, Goethe University Frankfurt, Theodor-Stern-Kai 7, 60590 Frankfurt am Main, Germany.

[3]IMPRS on Cellular Biophysics, 60438 Frankfurt, Germany

[4]Max Planck Institute for Brain Research, Frankfurt 60438, Germany

[5]Max Planck Institute of Biophysics, Frankfurt 60438, Germany

[6]Buchmann Institute for Molecular Life Sciences, Goethe University Frankfurt, Max-von-Laue Straße 15, 60438 Frankfurt am Main, Germany.

[7]Fraunhofer Institute of Translational Medicine and Pharmacology, Carl-von-Noorden-Platz 9, 60596 Frankfurt am Main, Germany

*A.B., C.O and P.M. contributed equally to this work
[#]Correspondence: osterburg@bpc.uni-frankfurt.de, *vdoetsch@em.uni-frankfurt.de*

Keywords: p53 isoforms; p53 family; aggregation

Abbreviations: TAD, transactivation domain; DBD, DNA binding domain; OD, oligomerization domain; RE, response element;

Abstract

The p53 transcription factor family consists of the three members p53, p63 and p73. Both p63 and p73 exist in different isoforms that are well characterized. Isoforms have also been identified for p53 and it has been proposed that they are responsible for increased cancer metastasis. In contrast to the p63 and p73 isoforms, which do not contain truncations in folded domains, most of the p53 isoforms contain only parts of either the DNA binding domain or the oligomerization domain. To better understand the effect of p53 isoforms in cancer we provide here a comprehensive biochemical characterization. With the exception of the Δ40p53α isoform none of the other variants can bind to DNA with high affinity and none can upregulate transcription. Probing with antibodies, DARPins and other interaction partners confirmed that isoforms harboring deletions in the DNA binding domain cannot interact specifically with them, but instead are bound to chaperones and other factors known to interact with misfolded proteins. Expression of isoforms with deletions in the DNA binding domain results in upregulation of cellular chaperones. If the expression level surpasses a threshold, the chaperone system can no longer keep these isoforms soluble resulting in aggregation and co-aggregation with other factors.

Introduction

The tumor suppressor p53 is the most mutated protein in cancer cells with more than 2000 different mutations identified so far (1,2). In tumor cells with wild type p53, its activity is also inhibited e.g. by the overexpression of E3 ligases such as Mdm2 (3,4). p53 is a transcription factor that sequence-specifically binds to DNA to regulate the transcription of genes involved in apoptosis and cell cycle inhibition as the two most direct processes that prevent tumorigenesis. In addition, p53 also regulates genes involved in many other processes such as DNA repair and metabolism. Structurally it consists of a central DNA binding domain (DBD), an N-terminal transactivation domain (TAD) and a C-terminal oligomerization domain (OD) through which it forms tetramers (5). At the very C-terminus an additional regulatory domain (CTD) is located, that binds unspecifically to DNA and contains multiple sites for phosphorylation, ubiquitination and other posttranslational modifications. Mutations can occur in all these domains but mainly cluster in the DBD (1,2). High affinity DNA binding requires the formation of tetramers which enables dominant negative effects of cancer mutations in the DBD as mutant p53 and wild type p53 can form mixed tetramers via their ODs with strongly reduced binding affinity. Similar dominant negative effects are known from the p53 family member p63 in which mutations in the DBD result in developmental defects based on a dominant negative mechanism (6,7). The discovery of p63 and the third family member p73 has revealed that these two proteins exist in multiple different isoforms that are created by the combination of different promotors with splicing events in the C-terminus which strongly influences the transcriptional activity of these isoforms (8). Different isoforms have also been identified for p53 (9) and it has been proposed that these isoforms are responsible for increased cancer metastasis as well as premature aging upon dysregulation. In contrast to the p63 and p73 isoforms, which do not contain truncations in folded domains, most of the isoforms of p53 contain only parts of either the DBD or the OD. All these deletions have strong effects on the biochemical behaviour of the isoforms (9,10). A deletion of the OD not only prevents the formation of tetramers which are required for high affinity DNA binding, it also deletes the nuclear export signal thereby influencing the subcellular localization of these isoforms. The wild type p53 DBD is known to be only metastable with a melting temperature of ~43°C (1,11). Many p53 mutations found in tumors destabilize the DBD further, resulting in unfolding and due to the exposure of aggregation prone peptide sequences in gain of function effects via co-aggregation with other cellular factors (12,13). This metastability combined with the in general cooperative folding behaviour of single domain proteins strongly predicts that the isoforms containing a truncated DBD cannot properly fold but have a high aggregation potential, similar to mutant p53 with destabilizing mutations.

p53 isoforms have been studied in different cellular systems and individual isoforms have been assigned specific regulatory functions (14-22). However, a comprehensive biochemical

characterization of these isoforms is missing and we propose that many of the observed effects can be assigned to co-aggregation of these isoforms with wild type p53 as well as other cellular factors such as the other members of the p53 protein family. Here we report a comprehensive characterization of the p53 isoforms with respect to their stability, DNA binding affinity, interaction with chaperones, aggregation and co-aggregation.

Results

All isoforms except wtp53 show a low to none transcriptional activity

So far, a total of 14 p53 isoforms with various truncations have been identified. Compared to the wild type p53 form (from now on named wtp53) alternative translation start sites create the isoforms Δ40p53, Δ133p53, and Δ160p53, each lacking the indicated number of amino acids from the N-terminus (23). The Δ40p53 variants have a deletion of the first 40 amino acids of the N-terminus including the transactivation domain 1 (TAD1) (24) but contain a wild type DBD and OD. The Δ133p53 and Δ160p53 isoforms lack in addition to the complete TAD parts of the DBD. These different N-terminal isoforms can be combined with three different C-termini called α, β and γ. Only the wild type α-C-terminus contains a full OD, the β- and γ-C-termini have a truncated OD with isoform specific extensions. Furthermore, two isoforms with C-terminal deletions of parts of the DBD (TAΔp53α) (25) and additional deletion of the remaining C-terminus including the entire OD (TAp53ψ) (26) have been described. Figure 1 shows an overview of all these isoforms.

As an initial experiment, we determined the transcriptional activity of the p53-isoforms in relation to wtp53 and different classes of p53 mutants both in H1299 and in SAOS-2 cells using reporter plasmids containing either the multiple repeats of a p53 RE (pBDS), p21 or Mdm2 promoters. All three promoters are very sensitive to p53. Hence, p53 isoforms which show weak or no response in luciferase assays, probably will not show any activity under endogenous protein expression levels on genomic promoters. To exclude the possibility that lower p53 isoform activities are due to reduced expression levels, a titration series with increasing amounts of wtp53 plasmid DNA was measured for comparison. In addition, we investigated artificial constructs that contained various combinations of full-length domains (DBD-OD-CTD; TA-DBD-OD; TA-DBD). wt-p53 showed a strong transcriptional activity (Figure 2A-C, Supplementary Figure S1A-C). An even higher activity was seen for the artificial construct TA-DBD-OD, lacking the CTD. As a negative control we used the p53R175H mutant,

which harbours a structural DBD mutation leading to a complete loss of transcriptional activity. TAp53β and TAp53γ still contain the full-length TA and DBD domains but lack the OD and therefore are unable to form tetramers. They showed a slight transactivation capacity, which is, however, several fold lower than the wtp53 activity. This slight capacity could be due to weak binding of the p53 monomers to DNA and their intact TA domain since isolated p53 DBDs can still cooperatively bind DNA with low affinity. This result is also consistent with the activity seen for the artificial TA-DBD construct. In agreement with a previous study (27) no transactivation capacity was detected for TAΔp53α which lacks part of its DBD and linker region to its OD as well as the nuclear localization signal (NLS) and for the p53ψ isoform (Figure 2D, Supplementary Figure S1D). Δ40p53α and Δ40p53β showed a slight transactivation capacity (100 to 200-fold below wt-p53). Δ40p53α lacks part of its TAD but preserves its OD while Δ40p53β lacks part of its TAD as well as of its OD domains. The artificial construct DBD-OD-CTD had a lower activity, as it lacks the TAD completely, while the TAD2 part is still present in the Δ40 isoforms (8,24). The other N-terminal truncations (Δ133 and Δ160) showed no activity at all, independent of their C-terminus (α, β, γ), consistent with a lack of the entire TAD and parts of the DBD as well as depending on the C-terminus a lack of the OD (Figure 2A-C).

The expression levels of the constructs differed with β-isoforms being much stronger expressed compared to α-isoforms (Supplementary Figure S1A-D). The γ-isoforms showed the lowest expression of all C-terminal truncations, while the lowest expression levels among the N-terminal isoforms was seen for the Δ133p53-isoforms. These data also demonstrated that the lowest wtp53 concentration had a much higher transcriptional activity compared to all other p53 isoforms, even when these isoforms reached concentrations many times above the concentration of wtp53. Taken together, some p53 isoforms showed a higher transactivation capacity compared to others, but no isoform reached the level of wtp53. Moreover, the titration series with wtp53 indicated that saturation in this assay is achieved above transfection with 50 ng plasmid. As we had used 267 ng for all isoforms, any remaining transcriptional activity should have been detected in this assay.

Only wtp53 and Δ40p53α bind DNA in pull-down assays

Next, we investigated the ability of the various p53 isoforms to bind to DNA using a pulldown experiment with the response elements (RE) of the p21 and the PUMA promoter. Only wtp53 and Δ40p53α showed binding to the p53-REs (Figure 2E, Supplementary Figure S1E). For high affinity DNA binding, p53 family members need a folded DBD and the ability to form tetramers. This requirement is met only by wtp53 and Δ40p53α. As a negative control we used again the p53αR175H mutant which is unable to bind DNA due to its destabilized DBD. For all other p53 isoforms no DNA binding could be observed due to the lack of a folded DBD (Δ133,

Δ160 constructs and p53ψ), lack of a functional OD (β- and ɣ-C-termini) or a combination of both. We confirmed the results of these pulldown assays for Δ40p53β by surface plasmon resonance (SPR) measurements with the p21 RE being immobilized on the chip (Figure 2F, Supplementary Figure S1F-H). The artificial DBD-OD construct showed high affinity while the affinity for the Δ40p53β was ~280-fold lower and comparable to the affinity of the isolated p53 DBD (Supplementary Figure S1H). For all other p53 isoforms SPR measurements were not feasible because these proteins could not be purified following bacterial expression. Summarizing the transactivation and DNA binding assays, all p53 isoforms show a behaviour more comparable to mutant p53 than to wtp53. Only Δ40p53α is able to bind DNA without exhibiting a significant transcriptional activity.

Only wtp53 and Δ40p53 isoforms have an intact DBD

We further investigated the integrity of the DBD with binding to different interaction partners – the Human Papilloma Virus (HPV) E6 protein, a recently described DARPin and the pAB240 antibody - that probe different interfaces. The E6 protein binds to a region of the p53 DBD different from the DNA binding interface (Figure 3A) and initiates the degradation of p53 by the ubiquitin proteasome system (28-30). Degradation requires the recognition of the p53 DBD by the E6 protein, an unfolded DBD or a DBD with a non-wild-type conformation does not get degraded. We expressed various p53 isoforms in rabbit reticulate lysate and determined the levels of the isoforms four hours after the addition of bacterially expressed GST-E6 protein or GST as control. As expected, wtp53 was completely degraded in this assay (Figure 3B, Supplementary Figure S2A). The structural mutant p53R175H was only partially degraded. This mutation locally perturbs the structure of the DBD, but also reduces the overall thermodynamically stability. Another structural mutant V157F was not degraded at all. The R273H mutation that is located in the DNA binding interface did not inhibit degradation demonstrating that it retains the wild-type fold of the DBD. TAp53ψ and TAΔp53α showed no decreased signal in the presence of HPV E6. Both lack C-terminal parts of the DBD, indicating that these isoforms are not able to fold their DBD correctly.

Isoforms that contain a complete DBD should be sensitive to this degradation assay and consequently, TAp53β, TAp53ɣ as well as Δ40p53β and Δ40p53ɣ are degraded, although not as efficiently as wtp53. This is consistent with a similar result for the artificial construct TA-DBD. A less efficient degradation might not directly reflect binding differences in the binding efficiency of the E6 protein but also differences in the accessibility of lysine residues necessary for ubiquitination. This effect can be seen in the less efficient degradation of the TAp53αΔCTD construct in which the lysine-rich CTD is missing (Figure 3B). The remaining p53 isoforms with deletions in the DBD (Δ133p53α-γ and Δ160p53α-γ) show only low levels or even no

degradation, similar to ΔNp63α which we have added as a negative control. While the explanation for the insensitivity of the Δ133p53 and Δ160p53 isoforms is that the missing parts of the DBD include part of the binding interface of the E6 protein, this interface is in principle present in the TAp53ψ and TAΔp53α isoforms. Their resistance to degradation shows that the remaining DBD does not adopt a fold that can be recognized by the E6 protein.

As a further experiment to investigate the conformational state of the DBD we probed isoforms expressed in H1299 cells by immunoprecipitation with the pAB240 antibody (Figure 3C, Supplementary Figure S2B). This antibody detects an epitope in the p53 DBD that becomes accessible only upon unfolding of the domain. The results showed that the two p53 mutants R175H and V157F were efficiently immunoprecipitated. Likewise, all Δ133 and in particular all Δ160 isoforms as well as p53ψ and TAΔp53α interacted with this antibody.

Finally, to investigate the structural integrity of the DBD we performed binding studies with the DARPin G4 which we had previously shown to bind to the DNA binding interface of p53 (31). For pulldown experiments we bound the biotinylated DARPin to Streptavidin beads and expressed different p53 isoforms and mutants either in rabbit reticulate lysate (Figure 3D, Supplementary Figure S2C) or in H1299 cells (Figure 3E, Supplementary Figure S2D) (Δ40p53 and Δ160p53 isoforms were not further tested as the first ones contain a fully folded DBD and results with Δ133p53 are directly transferable to Δ160p53). The G4 DARPin pulled down wtp53 as well as the R273H mutant. The R175H mutant was also pulled down, albeit with a lower efficiency with H1299 cells expressed protein. The efficiency for the V157F mutant was very low. None of the Δ133 isoforms or the p53ψ and TAΔp53α showed interaction.

Together, these binding studies demonstrated that only wtp53 and the Δ40p53 variants contain a fully folded DBD. High affinity DNA binding in addition requires a functional OD which enables only wtp53 and Δ40p53α to interact strongly.

The γ-C-terminus and isoforms with truncated DBDs exhibit a high aggregation propensity *in-silico*, *in-vitro* and *in-cellulo*

The only partial folding of many of the p53 isoforms triggered the question whether the unfolded state of the DBD and OD leads to changes in the solubility within the cell. The DBD contains an aggregation prone peptide sequence that is usually hidden within the folded structure but gets exposed upon unfolding (32). In case of p63, we had previously shown that mutations within the SAM domain also led to the exposure of a usually hidden aggregation prone peptide which results in aggregation of p63 (33) as the cause of the ankyloblepharon-ectodermaldefects-cleft lip/palate (AEC) syndrome, in human patients (34). In addition to point mutations in the SAM domain, also frame shift mutations cause the AEC syndrome by creating new aggregation prone sequences (33). We investigated the potential for such newly formed

aggregation prone regions (APRs) in the sequences of the β- and ɣ- as well as the TAp53ψ isoforms by an *in-silico* prediction method using the TANGO algorithm (35). This analysis predicted indeed the presence of novel APRs in the DBD of TAp53ψ and the OD of p53ɣ (Figure 4A-C).

Experimentally, we investigated the aggregation behaviour of H1299 expressed p53 isoforms by analytical size exclusion chromatography. The results indicated a tetrameric state for wtp53 as well as for p53R273H and Δ40p53α (Figure 4D). The cancer mutant p53R175H showed a mixture of tetrameric protein and partial aggregation indicated by a shift to higher molecular weight. TAp53β and Δ40p53β showed a shift towards lower molecular weight, consistent with their inability to form tetramers while TAp53ɣ and Δ40p53ɣ exhibited additional aggregation behaviour. Of the Δ133 and Δ160 isoforms, the α-C-terminus showed only a slight aggregation tendency, while both β- and ɣ-C-termini displayed very strong aggregation, as did the TAp53Ψ and TAΔp53 isoforms.

We further investigated the behaviour of these isoforms (aggregation is independent of Myc-tag position (Supplementary Figure S3A)) by native PAGE with similar results, except that in this experimental setting also the Δ133p53α and Δ160p53α isoforms showed strong aggregation (Figure 4E, Supplementary Figure S3A-B). Finally, we determined the relative amounts of protein in the soluble and insoluble fraction after expression in H1299 cells. In this assay again all Δ133 and Δ160 isoforms were found to a large degree in the insoluble fraction (Figure 4F, Supplementary Figure S3C). Δ40p53ɣ was also mainly found in the pellet while TAp53ɣ was mainly soluble as were the TAp53ψ and TAΔp53 isoforms. As the ɣ-C-terminus seems to promote aggregation we measured the tendency of the dye Thioflavin T (ThT) (36) to bind to a peptide derived from the ɣ-C-terminus and compared it to a peptide derived from the β-C-terminus. Thioflavin T binding was confirmed for the ɣ-peptide, while the β-peptide did not show binding above the background level, suggesting that indeed the ɣ-C-terminus has a high aggregation propensity *in-vitro* and *in-cellulo* (Figure 4G).

Aggregation is a function of the sequence but also of the concentration. In a cellular system chaperones are present that keep proteins with open hydrophobic stretches soluble, prevent them from aggregation and if this is impossible, associated E3 ligases will degrade the misfolded protein. To test the dependence on the concentration we expressed several isoforms under a minimal CMV promotor (selected artificial promotor, p5RPU.Myc (37), was cloned into pcDNA3.1 plasmid) which results in reduced expression levels in H1299 cells. Using this system, also Δ133p53α,β could indeed be kept soluble (Supplementary Figure S3D), suggesting that aggregation will only become a problem if the expression level surpasses a certain threshold level. To further test this hypothesis, we overexpressed Δ40p53α, Δ133p53α and Δ133p53β under the strong promotor in H1299 cells and treated the cells with different

HSP70 and HSP90 inhibitors. No effect was seen for Δ40p53α which remained soluble. For both Δ133p53α and Δ133p53β, however, the percentage of the insoluble fraction increased relative to the treatment with only DMSO, suggesting that inhibition of chaperones results in increased aggregation (Supplementary Figure S3E-G).

Interaction with chaperones

The experiments described above suggested that chaperones are involved in keeping aggregation-prone p53 isoforms soluble. The characterization so far predicted that several of the p53 isoforms have exposed hydrophobic patches due to misfolding of the DBD or as part of isoform-specific new APRs. We tested the interaction of p53 isoforms with chaperones by transiently transfecting H1299 cells with the individual p53 isoforms and then immunoprecipitating endogenous HSC/HSP70. Western blot analysis with an α-Myc antibody was used to detect co-immunoprecipitation of the N-terminally myc-tagged p53 isoforms. A strong signal was detected for the cancer mutant p53V157F (Figure 5A, Supplementary Figure S4A). Further interactions were seen for Δ40p53ɣ, Δ133α,β,ɣ, TAp53ψ and TAΔp53. Only weak signals occurred for wtp53, Δ40p53α, Δ40p53β and p53R273H in agreement with the interpretation that these isoforms and mutants do not have accessible hydrophobic patches or APRs.

We wanted to further investigate if expression of p53 isoforms creates cellular stress and triggers the expression of chaperones. To study this question, we measured the transcriptional activity on a reporter plasmid expressing luciferase under an HSP70 promotor (Figure 5B, Supplementary Figure S4B, C) and expressed at the same time different p53 isoforms. If the expression of these isoforms induced cellular stress which would result in the upregulation of chaperone expression, an increase in the luciferase activity should be detectable. These experiments showed that expression of p53 isoforms containing a ɣ-C-terminus, as well as all Δ133p53 versions lead to a strong activation of the HSP70 promotor. Elevated levels were also detected for TAΔp53, p53R175H and p53V157F, but not for the DNA binding interface mutant p53R273H. In addition, we investigated the effect of the isoform-specific β- and ɣ-C-termini by fusing them to the protein Scarlet (38). We compared the activity on the HSP70 promotor in cells expressing these fusion proteins with the activity in cells expressing Scarlet itself. The results showed that the ɣ-C-terminus strongly induced activity, but not the β-C-terminus. Responsible for the aggregation promoting effect of the ɣ-C-terminus (which according to the Waltz predictor is potentially amyloidogenic (39)) is presumably its hydrophobic nature. To investigate this hypothesis, we created the Y327A, L330A, L334A and L336A mutations in the ɣ-C-terminus which indeed reduced the luciferase expression to background levels.

Overall, these results suggest that luciferase expression via the HSP70 promotor was induced by the overexpression of certain p53 isoforms, suggesting that their only partially folded state and/or open hydrophobic patches induce a cellular stress response. To exclude the possibility that the p53 isoforms induce luciferase expression by direct DNA binding (although our experiments described above already showed that only wtp53 and Δ40p53α can bind DNA strongly) we repeated the same experiments with a reporter plasmid having three copies of a heat-shock element (HSE) in front of a SV40 promotor and which therefore - in contrast to the full HSP70 promoter (40) - does not contain any p53 REs. These experiments confirmed the data obtained with the HSP70 promotor, strongly suggesting that it is the isoform induced cellular stress that triggers the expression of chaperones (Figure 5C).

We further investigated the interaction of selected p53 isoforms with chaperones by mass spectrometry-based proteomics. For this purpose, we created stable U2OS cell lines in which the isoforms were fused to the C-terminus of the TURBO-ID biotin ligase and their expression is under control of a Tet Response Element. After induction of expression of the isoforms (with tetracycline) and initiation of biotinylation, we isolated biotinylated proteins with streptavidin-coated magnetic beads and used a Q Exactive HF coupled to an easy nLC 1200 mass spectrometer (ThermoFisher Scientific) to analyse proteins that were in close proximity to these selected isoforms. The results were filtered for the terms “chaperone”, “unfolded binding” and “misfolded binding”. Figure 5D shows that all isoforms interact with a common set of proteins (Supplementary Table S1). In addition to this common set, TAp53β and Δ40p53α showed only very few additional interaction partners. This situation was very different for Δ133α, Δ133β and TAp53ɣ which all showed close proximity to many more proteins involved in binding to un- or misfolded proteins. These data further confirm that Δ133p53 isoforms and isoforms with a ɣ-C-terminus contain hydrophobic patches and that their expression triggers cellular stress.

p53 itself was one of the most prominent proteins found in the interactome of all five investigated isoforms (Supplementary Table 1). This is expected as the TurboID ligase was fused to the N-terminus of all isoforms, which results in efficient self-biotinylation. To investigate if these isoforms also interact with wild type p53, we focused a new mass spectrometry experiment on the identification of p53 peptides and analyzed the interactome data for peptide precursors that can be quantified only in wild type p53 but not in the specific isoform (Figure 5E-G and Supplementary Figure S5). For Δ133p53α we could quantify a peptide precursor between amino acids 102 and 110 that is highly likely to originate from wild type p53. This result is not surprising as Δ133p53α contains a full oligomerization domain capable of forming mixed tetramers with wild type p53. These peptides were absent or beyond the detection limit in the Δ133p53β sample, in line with the interpretation that this isoform

cannot hetero-oligomerize with wild type p53. Peptides spanning the region amino acids 319 to 333 were only quantified in samples of Δ40p53α and Δ133p53α which contain the full length oligomerization domain themselves, which makes it impossible to determine if these peptides originate from wild type p53 or from the investigated p53 isoform. For Δ133p53β, TAp53β and TAp53ɣ we did not find any peptides in this region (with the exception of a precursor of very low intensity in a single Δ133p53β sample), supporting the interpretation that these isoforms do not interact with wild type p53. For Δ40p53α no wild type peptides originating from the first 40 amino acids were detected despite the presence of a full oligomerization domain. Overall, these data show that Δ133p53α can form mixed tetramers and can thus act dominantly negative towards wild type p53.

Some p53 isoforms can inhibit wt-p53, p63 and p73 by different mechanisms

The tetrameric state of p53 is the basis for the dominant negative effect of cancer mutations that inactivate DNA binding. The incorporation of one or more mutated p53 monomers into the tetramer weakens the binding to DNA. We wanted to investigate how the co-expression of selected p53 isoforms affects the activity of wtp53, p73 and p63. Co-expression of known cancer mutants strongly inhibited the activity of wtp53 as expected as did co-expression of all α-isoforms (Figure 6A, Supplementary Figure S6A). Expression of the Δ40p53α isoform can inhibit the activity of wtp53 also by blocking DNA binding (promotor squelching). Without a full TAD, this isoform is transcriptionally strongly suppressed. Co-expression of any isoform that is incapable of forming tetramers did not show any inhibitory effect. This includes all β- and ɣ-C-termini regardless of the N-terminal version as well as p53ψ and TAΔp53α. The inability of TAΔp53α to inhibit wtp53 seems surprising as it contains a truncated DBD but a full-length OD, in principle allowing it to form mixed tetramers with wtp53 (41). However, the deleted sequence includes the nuclear localization signal of the protein, which traps this isoform in the cytoplasm and prevents a dominant negative effect as also previously described (27).

Previous studies had shown that p73 and p63 do not interact with p53 via their ODs (42,43) but form mixed p63/p73 tetramers with a tetramer built from a p63 dimer and a p73 dimer being the thermodynamically most stable species (44). Co-expression of TAp73α with ΔNp63α, a p63 isoform that lacks the transactivation domain and therefore shows very little transcriptional activity on most promotors, inhibits p73's activity, most likely by promotor-squelching as previously described (44) (Figure 6B, Supplementary Figure S6B). Co-expression with ΔNp63αR304W, a mutant form incapable of binding DNA, however, showed that inhibition can also be due to the formation of mixed tetramers with decreased DNA binding affinity. Co-expression with Δ40p53α again strongly inhibited the activity of TAp73α, not through formation of mixed tetramers but by promotor-squelching which could be confirmed from the inability of

a R273H mutant of Δ40p53α to inhibit p73. All other p53 isoforms tested had no effect, consistent with their inability to bind to DNA and replace p73. The only exceptions were the Δ133 isoforms that showed an intermediate degree of inhibition. In a previous study we had shown that the α-C-termini of p73α and p63α can confer co-aggregation with destabilized p53 cancer mutants such as p53R175H (45). To probe if the observed inhibition by the Δ133 isoforms could be due to co-aggregation with this α-C-terminus we repeated the experiments with TAp73β which lacks this aggregation-prone sequences. The results mirror the data obtained with TAp73α with the exception that the inhibitory effect of the Δ133p53 isoforms was indeed strongly reduced (Figure 6C, Supplementary Figure S6C).

We also investigated the effect of p53 isoforms on p63's activity. As TAp63α forms inactive dimers (46), we used TAp63ɣ, a constitutive tetrameric and active isoform (47). The results are very similar to the data obtained with TAp73β, showing an inhibitory effect through promotor squelching only for Δ40p53α (Figure 6D, Supplementary Figure S6D). We further confirmed the interpretation that promotor squelching is the relevant mechanism by measuring the transcriptional activity of TAp63ɣ in the presence of increasing amounts of Δ40p53α which resulted in a concentration dependent inhibition. The presence of Δ40p53α harboring mutations in the DBD that inhibit DNA binding did not affect the transcriptional activity of TAp63ɣ (Figure 6E).

Finally, we used co-immunoprecipitation to investigate direct physical interactions between selected p53 isoforms and wtp53, p63 and p73. We transfected H1299 cells transiently with N-terminally HA-tagged p53, p63 or p73 isoforms and with N-terminally Myc-tagged p53 variants (Δ40p53α, Δ40p53β, Δ133p53α and Δ133p53β). p53, p63, or p73 isoforms were immunoprecipitated (IP) with an α-HA antibody and co-immunoprecipitation of p53 variants was probed with Western blots using an α-myc antibody (Figure 6F). Δ40p53α interacted strongly with wtp53 as well as with the p53R175H and p53R273H cancer mutants while Δ40p53β interacted weakly only with p53R175H, suggesting that these interactions are mediated by the OD. Similarly, interaction with all three p53 variants resulted in co-IPs with Δ133p53α. Interaction with wtp53 was weakest, showing that Δ133p53α can drag wtp53 into insoluble aggregates, but not very efficiently. Of the Δ133p53β co-IPs the strongest was with the p53R175H cancer mutant which forms co-aggregates. For p63 we tested the dimeric TAp63α, the open tetrameric ΔNp63α and the ΔNp63αV603D version in which the aggregation prone C-terminus is mutated to reduce the aggregation propensity (45). None of them showed interaction with Δ40p53α or Δ40p53β. The same was true for the co-IP with Δ133p53α. A co-IP could, however, be detected for ΔNp63α and Δ133p53β, which could be reduced by the V603D mutation in the p63 C-terminus, showing that this interaction is based on co-aggregation. Virtually the same results were obtained with co-IP experiments with different p73

isoforms. TAp73α which is a constitutively open and tetrameric isoform (48) shows co-aggregation with Δ133p53α and Δ133p53β which can get reduced by a V586D mutation in the α-C-terminus that reduces the aggregation propensity (45). Likewise, TAp73β which lacks the α-C-terminus shows a strongly reduced co-IP.

Discussion

The p53 protein family plays very important roles in genetic quality control, developmental programs and in tumor suppression (49). The discovery of p63 and p73 has shown that both proteins can exist in many different isoforms. In case of p63, very clear biological functions have been assigned to two of these, namely ΔNp63α which plays an important role in organizing the chromatin landscape in the basal cells of epithelial tissues (47,50) and TAp63α which is a crucial factor for maintaining the genetic quality in oocytes (46,51). For p73 functions in the development and maintenance of neurons, the development of ciliated cells (52) and in tumor suppression (53) have been described involving both TA- and ΔN-isoforms with the α- and the β-C-termini. Characteristic for these isoforms is that they contain fully folded domains and differ only in the complete absence or presence of such domains. The p53 isoforms show a different picture. With the exception of Δ40p53α which lacks parts of the unstructured transactivation domain, all are characterized by containing only parts of the DBD and/or the OD. As protein folding of single domains is in general a cooperative process, this predicts that these domains with missing secondary structure elements are largely unfolded and not capable of fulfilling a normal cellular function. Here we have used multiple experiments to provide a comprehensive characterization of these p53 isoforms. Our data demonstrate that high affinity DNA binding requires both a folded DBD as well as a folded OD. Only Δ40p53α fulfills these requirements and might have its own meaningful biological function, potentially as a transcriptional inhibitor of wtp53, similar to ΔNp63 and ΔNp73 isoforms which can inhibit wtp53 by promotor squelching. The potential role of Δ40p53α could be that of fine tuning of wtp53's activity as the formation of hetero-complexes with a reduced number of TADs influences not only the transcriptional activity directly but potentially also indirectly as a reduced number of TADs can reduce the Mdm2 dependent degradation rate. This can lead to an even increased overall transcriptional activity as shown for titrations of TAp63 and ΔNp63 isoforms (47). All other p53 isoforms do not bind strongly to DNA either due to lack of a functional DBD, a functional OD or even both. Instead, the unfolded / partial folded states, in particular of the DBD, as well as the hydrophobic nature of the ɣ-C-terminus increase cellular stress as evidenced by the upregulation of chaperones and the association of chaperones and proteins involved in interaction with unfolded/misfolded proteins with these isoforms. Below a certain expression level the cellular chaperone systems seem to be able to keep these isoforms

soluble but above this level they accumulate in insoluble aggregates. While the lack of crucial functional domains prevents well defined physiological roles of these isoforms (with the potential exception of Δ40p53α as mentioned above), they have the potential to inactivate members of the p53 protein family by forming inactive hetero-complexes with wtp53 (Δ133p53α, Δ160p53α), by direct co-aggregation with α-isoforms of p63 and p73 (Δ133p53α,β,ɣ and Δ160p53α,β,ɣ) or promotor squelching (Δ40p53α). The exception from this rule is TAΔp53α, which aggregates (41) and could in theory bind to wtp53 via its OD, but lacks an NLS and therefore cannot be imported in the nucleus to execute its dominant negative effect. Forced translocation of TAΔp53α into the nucleus was shown to establish a dominant negative effect, demonstrating that the lack of the NLS is the main impairment of a negative effect on wtp53 (27). The potential interaction mechanisms of p53 isoforms with members of the p53 family are summarized in Figure 7.

Through these mechanisms expression of many of the p53 isoforms can have detrimental effects and the literature on these isoforms so far shows a clear correlation with cancer. The least effect is to be expected from Δ40p53β which is only little more than an isolated p53 DBD and Δ40p53ɣ. This isoform, however, has the ability to aggregate and co-aggregate with other proteins due to the very hydrophobic nature of the ɣ-C-terminus. For all other isoforms severe effects – increasing with the cellular concentration – can be expected. Depending on in which cell types this expression occurs, different overall physiological effects (cancer, neurodegeneration) can result. While this study is focused on the effects that truncations have on the folded domains of p53, it should be mentioned that deletion of the unfolded N-terminal as well as C-terminal domains also impairs the normal function of p53 (54). These domains are the target of a large number of posttranslational modifications and are important for the interaction with regulatory proteins, for example p300 and Mdm2 in the transactivation domain.

The aggregation potential of many of the p53 isoforms has been noticed in several other publications as well. The lab of Curtis Harris has shown by mass spectrometry analysis following co-immunoprecipitation of FLAG-tagged Δ133p53α in MRC-5 fibroblasts that Δ133p53α interacts with members of the Hsp70 chaperone families as well as the chaperone-associated E3 ubiquitin ligase STUB1 as well as BAG2 and BAG5 (15), similar to our Turbo-ID based proteomics study reported here (Figure 5D). Moreover, Vieler *et al.* stated that they observed increased aggregation of Δ133p53 without presenting any data (55), whereas a computational study of the Δ133p53 DBD suggested a lower stability correlated with a high tendency for aggregation (56). Experimentally, the aggregation behavior of Δ133p53β has been investigated by Arsic *et al.* (57). They also found that this isoform interacts with the CCT chaperone complex and that depletion of this complex further promotes aggregation. Direct experimental evidence for the instability and aggregation tendency of the TAΔp53 isoform was

provided by the Fersht laboratory (41). They confirmed that this isoform cannot bind to the p21 promotor and in mixed states significantly reduces the DNA binding affinity of wtp53.

All the data suggesting that deletion of parts of the DBD result in the inability to bind DNA, the exposure of aggregation prone peptide sequences and aggregation as well as co-aggregation with other cellular factors are supported by a large literature on the effect of structural mutations in the p53 DBD. Numerous studies have shown that the only metastable DBD of p53 gets further destabilized by these mutations leading to loss of DNA binding and aggregation behavior (12,32). If single point mutations in the DBD can have that strong effects, it is more than likely that deletions of entire parts of the domain will have even stronger effects – consistent with all the data reported here.

In conclusion, the effects seen in cell culture as well as in patients with overexpression of different p53 isoforms should be interpreted on the background of the aggregation propensity as well as a potential overload of the cellular chaperone system instead of any specific interaction of these isoforms with proteins or DNA.

Material and Methods

Molecular Cloning

For transient protein expression in mammalian cells or *in-vitro* translation of N-terminally Myc-, HA- or Flag-tagged p53, p63 and p73, PCR-generated inserts were introduced in pcDNA3.Myc, p5RPU.Myc, pcDNA3.HA or pcDNA3.Flag, respectively, by subcloning using BamHI and XhoI restriction sites. pcDNA3.Myc, pcDNA3.HA or pcDNA3.Flag are derivatives of pcDNA3.1(+) (Thermo Fisher Scientific) engineered with a Myc, HA- or Flag-tag between HindIII and BamHI sites. pcDNA3.Myc was further modified by exchanging the CMV-promoter with a synthetic minimal promoter 5RPU (37) yielding p5RPU.Myc. All inserts lack the intrinsic start codon to avoid expression of untagged proteins via alternative translation initiation skipping the respective tag. For the p53 isoform inserts full-length TAp53α cDNA was used as a template with the isoform-specific β-, γ- and ψ-C-termini sequences being added via the 3'-oligo. The deletion in the Δp53 isoform as well as any mutations were generated by site-directed mutagenesis. For the C-terminally Myc-tag p53 isoforms, PCR-generated inserts were subcloned in the pcDNA3.1(+) via BamHI and XhoI restriction sites with a Kozak-sequence and start-codon being added by the 5'-oligo and the Myc-tag by the 3'-oligo.

For the generation of stable cell lines expressing p53 isoform N-terminally fused to Myc-tag and TurboID, PCR-generated p53 inserts were introduced in pTurboN by subcloning using BamHI and XhoI restriction sites. pTurboN was created by inserting a Myc-tag followed by

TurboID in pcDNA5/FRT/TO (Thermo Fisher) via the HindIII and BamHI restriction sites. V5-TurboID-NES_pCDNA3 (a gift from Alice Ting (Addgene plasmid #107169; http://n2t.net/addgene:107169; RRID:Addgene_107169)) was used as a template and the Myc-tag was added via the 5'-oligo.

For luciferase reporter assays with the full HSP70 promoter or the heat shock elements (HSE) only, the HSP70 promoter (-775 to 214) or three repeats of the HSP70 promoter HSE (AGAACGTTCTAGAAC) were subcloned in the pGL3-Basic vector (Promega) using NheI and XhoI as restriction sites.

For recombinant expression of the thermostabilized (TS) variants of p53 DBD-OD (41-356), p53 DBD-OD (41-356), p53 DBD (41-312) and Δ40p53beta in *E. coli*, inserts were generated by PCR using a p53 template carrying four thermostabilizing mutations (M133L V203A N239Y N268D) (1) and introduced in pET-15b-His_{10}-TEV (N-terminal His_{10}-tag followed by TEV protease cleavage site (MGHHHHHHHHHHDYDIPTTENLYFQGS), previously described in (6) by subcloning using BamHI and XhoI restriction sites.

For expression of the HPV16 E6 (AA9-158), an insert were generated by PCR using p3036 GST-HPV-16 E6 (a gift from Peter Howley (Addgene plasmid #10849; http://n2t.net/addgene:10849; RRID:Addgene_10849)) as a template. The insert was subcloned in pGEX-His8-TEV using BamHI and XhoI restriction sites. pGEX-His8-TEV was created by exchanging the 3C protease cleavage site (…GDHPPKSDLEVLFQGPLGS…) in pGEX-6P-2 (Cytvia) with a His8-tag followed by a TEV protease cleavage site (…GDHPPGTHHHHHHHHPGTENLYFQGS…). For the expression of GST only, a stop-codon was inserted in pGEX-His8-TEV using BamHI and XhoI restriction sites.

The cloning of the expression plasmids for the p53 family DBD-specific DARPin G4 and the non-binding control DARPin (cDP) has been previously described (31).

Protein expression and purification

For protein production *E. coli* BL21(DE3) Rosetta cells (SGC Frankfurt) were transformed with the respective *E. coli* expression plasmid. Cells were grown at 37 °C in 2xYT medium to an optical density (OD) of ~0.8 and protein expression was induced with 1 mM IPTG (Carl Roth) for 16-18 h at 18 °C, except for GST only which was expressed at 22 °C. For p53 variants and HPV16 E6 the medium was additionally supplemented with 100 µM zinc acetate (Carl Roth). After expression was completed, cells were harvested by centrifugation and the pellet was snap frozen in liquid nitrogen and stored at -80 °C until use.

For purification the cell pellet was thawed on ice and resuspended in IMAC A buffer (25 mM HEPES pH 7.2, 400 mM NaCl, 5% Glycerol, 20 mM β-ME,10 µM zinc acetate and 25 mM imidazole) supplemented with DNAse (Sigma-Aldrich), RNAse (Sigma-Aldrich) and self-

prepared protease inhibitor. After cell lysis by sonification, the lysate was cleared by centrifugation at 4 °C. All proteins were subjected to an initial immobilized metal affinity chromatography (IMAC) purification step. The supernatant was loaded onto HiTrap IMAC Sepharose FF column (Cytiva) pre-equilibrated in IMAC A buffer, bound proteins were washed with 20 column volumes (CV) IMAC A buffer and eluted with 2 CV IMAC B buffer (IMAC A with 300 mM imidazole). The eluted proteins were then further processed in different ways. All p53 variants were supplemented with self-prepared TEV protease (1:50 w/w) for removal of the His-tag and dialysed against IMAC A buffer overnight (ON) at 4 °C. A subsequent reverse IMAC step was performed to remove TEV protease, the cleaved tag and any uncleaved protein. p53 variants were further purified by heparin-based affinity/ion-exchange (IEX) chromatography. Prior loading on HiTrap Heparin HP columns (Cytiva), the salt concentration of the protein solutions was reduced below 100 mM by dilution with IEX A buffer (25 mM HEPES pH 7.2, 50 mM NaCl, 5% Glycerol, 20 mM β-ME,10 µM zinc acetate). Bound protein was eluted with a gradient from 50 mM to 1 M NaCl over 20 CV using IEX B buffer (IEX A with 1 M NaCl). In a final polishing step, p53 proteins were subjected to size exclusion chromatography (SEC) using a self-packed Superdex 200 SEC column (Cytiva) equilibrated in p53 storage buffer (25 mM HEPES pH 7.5, 150 mM NaCl, 0.5 mM TCEP). Monodisperse peak fractions were pooled, concentrated by centrifugation (Amicon Ultra Centrifugal Filters, Merck KGaA) and snap frozen in liquid nitrogen for storage at -80 °C until usage.

GST-HPV16 E6 and GST were further purified by glutathione affinity chromatography (GAC) after IMAC instead. The proteins were loaded onto a GSTrap FF Columns column (Cytiva) pre-equilibrated in IMAC A buffer, bound proteins were washed with 20 column volumes (CV) IMAC A buffer and eluted with 2 CV GAC buffer (IMAC A with 20 mM reduced glutathione instead of imidazole). GST was then subjected SEC using a self-packed Superdex 75 SEC column (Cytiva) equilibrated in GST storage buffer (25 mM HEPES pH 7.5, 150 mM NaCl, 10% glycerol, 0.5 mM TCEP). Monodisperse peak fractions were pooled, concentrated and stored as described above. As GST-HPV16 E6 aggregates at high concentrations, following GAC the protein was only subjected to a salt exchange using HiTrap Desalting columns with Sephadex G-25 resin (Cytvia) equilibrated in GST storage buffer and directly frozen and stored at described above.

The biotinylated p53 family DBD-specific DARPin G4 and the non-binding control DARPin (cDP) were expressed and purified as previously described (31).

Analytical SEC of purified proteins

Analytical SEC of purified proteins was performed operating a Superdex 10/300 GLwith an ÄKTA purifier chromatography system at 4 °C. SEC buffer (25 mM HEPES pH 7.5, 150 mM NaCl and 0.5 mM TCEP) was freshly prepared, filtered and degassed. Proteins were injected

on the SEC column equilibrated in the SEC buffer and elution was monitored via absorbance at 280 nm. For visualization of analytical SEC results, the absorbance signal was normalized and plotted against the elution volume (Prism 8).

Analytical SEC of cell lysates

Analytical SEC of cell lysates was performed operating a Superose 6 3.2/300 with an ÄKTA purifier chromatography system at 4 °C. The SEC buffer (50 mM TRIS pH 7.5, 150 mM NaCl, 20 mM CHAPS and 1 mM DTT) was freshly prepared, filtered and degassed. Cells were seeded in 6-well plates and transfected with cell culture expression plasmids encoding the respective proteins. 24 h after transfection, cells were harvested, resuspended in 120 µl analytical SEC lysis buffer (10 ml SEC buffer supplemented with 2 mM $MgCl_2$ and 1 tablet cOmplete, Mini, EDTA-free), immediately frozen in liquid nitrogen and stored at -80 °C until further use. Prior SEC analysis, cells were thawed in an ice-water bath, supplemented with 2 µl benzonase, incubated 60 min on ice and centrifuged for 15 min at 16,000 xg and 4 °C to remove cell debris. 50 µl supernatant was injected on the SEC column equilibrated in the SEC buffer and 85 µl fractions were collected in a 96-well microtiter plate. For subsequent WB analysis, 40 µl of the fractions were mixed with 10 µl 5x SDS-PAGE sample buffer in 96-well PCR plateand boiled for 5 min at 95°C

SPR

Specific DNA binding of recombinantly expressed and purified p53 constructs was measured by surface plasmon resonance (SPR) spectroscopy using a Biacore X-100 system (Cytiva). The protocol was adopted from Chen et al. (58) and has been performed as previously described by us for p53 and p63 (6,59).

Proteins were dialysed overnight at 4°C against SPR buffer (25 mM HEPES pH 7.5, 200 mM NaCl, 0.5 mM TCEP and 0.005% Tween-20) and centrifuged to remove any aggregates. For the measurements, protein solutions were prepared by serial dilution (factor 2-2.5). Approximately 200 response units (RU) of biotinylated annealed dsDNA with the 20 bp p21 RE was immobilized in flow cell F2 of an SA chip (Cytiva) and an equal amount of the dsDNA with a random sequence in flow cell F1. All measurements were conducted at 20 °C and in the multi-cycle format with at least one start-up cycle followed by nine measurement cycles with increasing protein concentrations. Each cycle comprised a 3 min association phase followed by a 2 min dissociation phase. The surface was regenerated by two consecutive 15 s injections of SPR regeneration buffer (25 mM HEPES pH7.5, 500 mM NaCl, 0.05% SDS). All measurements were performed consecutively with the same chip in three replicates of independently prepared dilution series.

Sensograms were background corrected and affinity binding curves were extracted by equilibrium analysis using the the BIAevaluation software (Cytiva). Affinity curves were plotted and fitted with a non-linear, least squares regression using a single-exponential one-site binding model with Hill slope to determine the dissociation constant K_D, the Bmax value and Hill slope factor h (Graphpad Prism 8).

Thioflavin T assay

Thioflavin T assay was performed using a Spark multimode microplate reader (Tecan) and Thioflavin T to determine aggregational behavior. Samples were prepared for measurement by mixing 10 µl of peptide stock solution (25 mM HEPES (pH7.5), 160 mM NaCl, 0.5 mM TCEP, 6 M GndHCl; final peptide concentration of 20 µM) and 0.1 µl Thioflavin T working solution (25 mM HEPES (pH 7.5), 150 mM NaCl, 0.5 mM TCEP; final ThT concentration of 25 µM) to a final volume of 200 µl in black, nonbinding polystyrol microplates (Greiner Bio-One). Prior to measuring the amyloid-specific fluorescent signal, the samples were incubated at 37 °C for 45 min. Measurements were performed using Ex: 430/20 and Em: 485/20 filters. Fluorescent signals were determined in three independent measurements from the same peptide batch. Statistical significance was assessed by ordinary one-way ANOVA using Graphpad Prism 8.

Cell culture

The non-small cell lung cancer cell line H1299 (purchased from ATCC) was used because of its p53 deletion and non-detectable or low endogenous levels of p63 and p73 (60), respectively, resulting in low background levels for the functional assays in this study. Cells were cultured at 37 °C and 5% CO_2 in RPMI 1640 medium (Thermo Fisher Scientific) supplemented with 10% Fetal Bovine Serum (FBS, Capricorn Scientific), 100 U/ml penicillin and 100 µg/ml streptomycin (Thermo Fisher Scientific). H1299 cells were routinely tested for mycoplasma contaminations.

For recombinant protein expression, H1299 cells in medium without antibiotics were transfected using Lipofectamine 2000 transfection reagent (Thermo Fisher Scientific) according to the manufacturer's recommendation.

Generation of stable cell lines

For generation of stable inducible expressing p53 isoform cell lines the U2OS Flp-In T-Rex cells (gift from C. Behrends, generated according to the protocol of Thermo Fisher Scientific) for homologous recombination of the target genes was used. After two weeks of culturing the T-Rex-U2OS cells were transfected in a six-well plate using the Lipofectamine 2000 transfection reagent (Thermo Fisher Scientific) with pcDNA5/FRT/TO (Thermo Fisher

Scientific) containing p53 family isoforms, as well as pOG44 (Thermo Fisher Scientific) containing the Flp recombinase according to the manufacturer's recommendations. After transfection, DMEM medium containing 10% tetracycline-free FBS (Bio Cell) was used. 24h after transfection cells were reseeded in 15cm dishes. One day after cell transfer the medium was exchanged to selection medium (10% tetracycline-free FBS, 4 µg/ml blasticidin, 200 µg/ml hygromycin (Thermo Fisher Scientific), 100 U/ml penicillin, 100 µg/ml Streptomycin and 1 mM pyruvate). Cells were cultured until a non-transfected control showed no viable cells (~10-14 days). Ten single colonies of each cell line were isolated, cultured and inducible expression of the desired proteins was tested via Western Blot. Protein expression was induced by adding 1 µg/mL tetracycline (Thermo Fisher Scientific) to the selection medium for 24h. For further experiments, three individual clones of each p53 family isoform were chosen.

Pulldown – Mass Spectrometry

To prepare proteomic samples for mass spectrometry analysis, stable cell lines expressing p53 variants were induced by adding 1 µg/mL tetracycline to selection medium for 24h. After induction, cells were collected and lysed on ice in RIPA lysis buffer (50 mM HEPES (pH 7.5), 150 mM NaCl, 1% Nonidet P-40, 1% sodium deoxycholate, 2 mM $MgCl_2$,1 mM DTT) with the addition of protease and phosphatase inhibitors. Lysates were sonicated and cleared by centrifugation. Afterwards, 100 µL lysate was taken out from the extracts and used to estimate the protein concentration with the Pierce™ BCA Protein Assay Kit (Thermo Fisher Scientific). To enrich biotinylated proteins from the protein extracts, 125 µL of streptavidin-coated magnetic beads (Dynabeads™ MyOne™ Streptavidin C1, Invitrogen) were washed 5x with wash buffer 1 (50 mM HEPES pH 7.5, 200 mM NaCl, 1 mM DTT, 0.1% Tween-20). Wash buffer 1 was exchanged from the beads with 1 mL protein lysate and incubated on a rotor overnight at 4 °C. The beads were sequentially washed 5x with 1 mL wash buffer 1 (50 mM HEPES pH 7.5, 200 mM NaCl, 1 mM DTT, 0.1% Tween-20) followed by five further wash steps with 1 mL wash buffer 2 (50 mM HEPES pH 7.5, 200 mM NaCl). To confirm the successful enrichment of the biotinylated proteins, 75 µL of the suspension were taken out for Western blot analysis and bound proteins were eluted with LDS buffer. The remaining liquid on MS samples was completely removed from the beads. Sample preparation for mass spectrometry was performed through on-bead digestion, employing a buffer containing 2% Sodium Deoxycholate, 1mM TCEP, and 4mM CAA, prepared in a 50 mM Tris pH 8.5. The Trypsin digestion process was carried out overnight, followed by sample purification using SDB-RPS membranes. Subsequently, the samples underwent a desalting step before being subjected to analysis on the mass spectrometer.

LC-MS analysis

Samples were analysed on a Q Exactive HF coupled to an easy nLC 1200 (ThermoFisher Scientific) using a 35 cm long, 75µm ID fused-silica column packed in house with 1.9 µm C18, and kept at 50°C using an integrated column oven. Peptides were eluted by a non-linear gradient from 4-32% acetonitrile over 60 minutes and directly sprayed into the mass-spectrometer equipped with a nanoFlex ion source (ThermoFisher Scientific). Full scan MS spectra (300-1650 m/z) were acquired in Profile mode at a resolution of 60,000 at m/z 200, a maximum injection time of 20 ms and an AGC target value of 3 x 106 charges. Up to 10 most intense peptides per full scan were isolated using a 1.4 Th window and fragmented using higher energy collisional dissociation (normalised collision energy of 27). MS/MS spectra were acquired in centroid mode with a resolution of 30,000, a maximum injection time of 54 ms and an AGC target value of 1 x 105. Single charged ions and ions with unassigned charge states were not considered for fragmentation and dynamic exclusion was set to 20s.

Mass spectrometry data processing

MS raw data processing was performed with MaxQuant and its in-build label-free quantification algorithm MaxLFQ applying default parameters (61). Acquired spectra were searched against the human reference proteome (Taxonomy ID 9606) downloaded from UniProt (21-11-2018; 94731 sequences including isoforms) and a collection of common contaminants (244 entries) using the Andromeda search engine integrated in MaxQuant (62). Identifications were filtered to obtain false discovery rates (FDR) below 1% for both peptide spectrum matches (PSM; minimum length of 7 amino acids) and proteins using a target-decoy strategy (63). Further statistical analysis was performed on Perseus software.

Sample processing for LC-MS/MS with a focus on p53-specific peptides

Eluted proteins (30 µg) were prepared for bottom-up proteomics using a suspension trapping protocol. Briefly, samples were mixed with lysis buffer (10% SDS, 100 mM tetraethylammonium bicarbonate (TEAB), pH 7.55, with H3PO4) in a 1:1 ratio, reduced using 20 mM dithiothreitol for 10 min at RT, and alkylated with 50 mM iodoacetamide for 30 min at RT in the dark. Subsequently, the samples were acidified using phosphoric acid in a final concentration of ~1.2%. Binding/wash buffer (BW: 90% methanol, 50 mM TEAB, pH 7.5 with H3PO4) was added in a 1:7 ratio. The protein suspension was loaded onto the S-trap filtered (size: “micro”; ProtiFi) by centrifugation for 20 s at 4000 x g. Trapped proteins were washed with 150 µl of BW buffer four times. Trypsin (1 µg; Promega) was added in 60 µl of 40 mM ammonium bicarbonate buffer. Digestion was performed overnight (~18 hours) at RT in a humidified chamber. Peptides were collected by washing in three consecutive steps by centrifugation at 4000 x g for 40 s starting with digestion buffer and two washes of 0.2% formic

acid in MS-grade water (H2O). Peptides were desalted using C18 SPE cartridges (25 mg, INSOLUTE EC, Biotage) and dried in vacuo at 45°C.

LC-MS/MS analysis of turboID experiment

Dried peptides were reconstituted in 20 µl reconstitution buffer (95% H2O, 5% acetonitrile (ACN) with 0.1% FA) and analyzed using a nanoElute 2 nano-HPLC coupled to a timsTOF HT mass spectrometer via a captive spray ion source (1600 V, Bruker Daltonics). Peptides were loaded directly onto the analytical column (15 cm × 150 µm column with 1.5 µm C18-beads (PepSep); at max. 800 bar) maintained at 60°C and connected to a 20 µm ZDV sprayer (Bruker Daltonics). In 25 min runs, peptides were separated in a linear gradient of water (buffer A: 100% H2O and 0.1% FA) and acetonitrile (buffer B: 100% ACN and 0.1% FA) ramping from 2% to 38% B in 21 min with a constant flow rate of 800 nl/min, followed by a wash of 95% B for 4 min with a flowrate of 1 µl/min. For data acquisition in DIA-mode, the 'short-gradient' dia-PASEF method was employed. In brief, 21 dia-PASEF windows were distributed to a TIMS scan each, covering a m/z-range from 475 to 1000 m/z in 25 Da DIA windows, resulting in an estimated cycle time of 0.95 sec. The ion mobility range was covered from 1.30 to 0.85 Vs/cm2. For further details, all method parameters are embedded in the uploaded raw data.

Processing of DIA LC-MS/MS data of turboID experiment

DIA-MS raw files were analyzed with the open-source software DIA-NN (version 1.9; "PMID: 31768060") using a library-free approach. The predicted library was generated using the in silico FASTA digest (Trypsin/P) option with the human UniProtKB database (swissprot, tremble, download: 08.05.2023). Common MS-contaminants were included in the search (Cambridge Centre for Proteomics (CCP) database). Deep learning-based spectra- and RT-prediction was enabled. The observed peptide length range was set to 7-35 amino acids, missed cleavages to 2 and precursor charge range to 1-5. N-terminal methionine excision, methionine oxidation, and N-terminal acetylation were set as variable modification, cysteine carbamidomethylation as a fixed modification. The number of variable modifications per peptide was limited to 3. MS1 and MS2 mass accuracies were set to 15 ppm. Precursor and run-specific protein group false-discovery rates (FDR) were filtered for hits <=1%. Scan-windows were set to 0, isotopologues were enabled, while the shared spectra option, match-between-runs, and LFQ normalization were disabled. Protein inference was performed using genes with the heuristic protein inference option enabled. The neural network classifier was set to single-pass mode and the selected quantification strategy was 'QuantUMS (high precision)'. The cross-run normalization was set to 'RT-dependent', the library generation to 'smart profiling', the speed and Ram usage to 'optimal results'. To evaluate protein-level LFQ data, the DIA-NN report table was imported in the statistical computing software R. Protein and

precursor output tables were analyzed in the statistical computing software R, filtering for proteotypicity and discarding contaminant hits. Using priniciple component analysis and unsupervised hierarchical clustering of Pearson correlation coefficients, four outlier samples were identified in an unbiased manner and thus removed from downstream analysis. All visualizations were performed using ggplot2 of the tidyverse R package.

Luciferase reporter assay

Transcriptional activity was analyzed via a reporter assay. H1299 cells were transfected with pRL-CMV (Promega) in combination with pBV-Luc BDS-2 3x WT (pBDS-2) (BDS-2 3x WT (p53 binding site) was a gift from Bert Vogelstein (Addgene plasmid #16515; http://n2t.net/addgene:16515; RRID:Addgene_16515)), pGL2 with Mdm2 promoter, pGL3 with p21 promoter(64), pGL3 with the HSP70 promoter or pGL3 with HSP70/3x heat shock elements (HSE), and pcDNA3.1(+) as an empty vector control or pcDNA3.Myc plasmids encoding the indicated Myc-tagged p53, p63 or p73 variants.

Cells were transfected one day after seeding. 24 h after transfection, cells were harvested and resuspended in 450 µL fresh medium. Per sample, 45 µl cell suspension was transferred in four wells each of a white Nunc 96-well microplates (Thermo Fisher Scientific) to determine the luciferase signal in technical quadruplicates.

Activities of Firefly and Renilla luciferase were measured with the Dual-Glo® Luciferase Assay System (Promega) according to the manufacturers' recommendation. Luminescence signals were measured using a Spark multimode or a GENios Pro microplate reader (Tecan). Analysis was performed by calculation of the ratio of luminescence from the experimental reporter (Firefly) to luminescence form the control reporter (Renilla) for each technical replicate and normalized to the empty vector control to yield the relative fold induction for each biological replicate. For further input sample preparation for Western blot analysis, the residual cells were centrifuged, resuspended in 150 µl 2x SDS-PAGE sample buffer and boiled.

SDS-PAGE and Western blotting

Proteins were separated by SDS-PAGE using Mini-PROTEAN Tetra Cell SDS-PAGE system (Bio-Rad) in combination 4–15% Mini-PROTEAN TGX Stain-Free Precast Protein gels (Bio-Rad). The SDS-PAGE gels were blotted onto PVDF membranes using the Trans-Blot Turbo Transfer System in combination with the Trans-Blot® Turbo™ RTA Midi PVDF Transfer Kit from Biorad and the SDS PAGE Transfer Buffer according to the manufacturer's recommendation. Membranes were incubated with blocking solution (5% skim milk powder (Sigma-Aldrich) in TBS-t (TBS supplemented with 0.05% (v/v) Tween 20)) for 1 h at room temperature under shaking conditions. Subsequently, the membranes were incubated with the

first antibody diluted in blocking solution overnight at 4 °C. Afterwards, the membrane was three times washed with TBS-t and incubated with the appropriate peroxidase-conjugated secondary antibody (Jackson ImmunoResearch) in blocking solution and washed three times again. The chemiluminescence signal was detected with a Lumi Imager F1 documentation system using Amersham ECL Prime WB Detection Reagent (Cytiva). Densitometric analysis of western blots was performed using ImageJ (Version 1.51) and/or using Bio-Rad ChemiDoc Image Lab 6.1. Statistical significance was assessed by ordinary one-way ANOVA followed by Tukey's post hoc test using Graphpad Prism 8.

The following primary antibodies were used in this study: anti-Myc (clone 4A6, Merck KGaA, 1:1000), anti-HA (goat polyclonal, Bethyl Laboratories, 1:1000), anti-p53 (DO-1, Santa Cruz Biotechnologies, 1:1000), anti-Vinculin (clone 7F9, Santa Cruz Biotechnology, 1:1000), anti-GST-HRP (GE Healthcare Life Sciences, 1:10000), anti-Streptavidin-HRP (Sigma-Aldrich Chemie GmbH, 1:10000), anti-Flag (M2 clone, Sigma-Aldrich Chemie GmbH, 1:1000), anti-HSP70/HSC70 (sc-24 clone, Santa Cruz Biotechnology, 1:1000).

Blue Native-PAGE

Blue Native(BN)-PAGE analysis to assess the oligomeric state and aggregation of p53 variants was performed as described previously (45). H1299 cells were harvested 24 h after transfection and lysed for 30 min at room temperature in 100 µl BN-PAGE lysis buffer (25 mM TRIS-HCl pH 7.5, 150 mM NaCl, 20 mM CHAPS, 1 mM DTT and 2 mM $MgCl_2$) supplemented with 1x protease inhibitor (Roche) and 1 µl benzonase (Merck). Samples were supplemented with 3x BN-PAGE solution (60% glycerol and 15 mM Coomassie Brilliant Blue G-250) and separated for 1 h at 150 V, followed by 1 h at 250 V, using the NativePAGE Bis-Tris Gel System with 3-12% Bis-Tris Mini Protein Gels (Thermo Fisher Scientific) at 4 °C. Subsequent immunoblotting and detection was performed using the XCell II blot system (Thermo Fisher Scientific) as described above with the exception that membranes were destained with methanol and fixed with 8% acetic acid before blocking. For parallel SDS-PAGE analysis, lysates were supplemented with 5x SDS-PAGE sample buffer (250 mM TRIS pH 8.0, 7.5% (w/v) SDS, 25% (v/v) glycerol, 0.025% (w/v) bromphenol blue sodium salt and 12.5% (v/v) β-ME), boiled and subjected to SDS-PAGE followed by immunoblotting as described above.

DNA pulldown assay

Per pulldown 50 pmol of biotinylated annealed p21 RE dsDNA oligonucleotide were immobilized on 10 µl MyOne T1 Dynabeads (Thermo Fisher) in DNA pulldown buffer (50 mM HEPES pH7.5; 200 mM NaCl; 0.1% Tween-20; 0.5 mM TCEP) for 1 h at 4°C. Myc-tagged p53 isoforms were produced by *in-vitro* translation (#L1170, Promega) from the respective pcDNA3.1(+) plasmids. Expression was conducted for 90 min at 30°C and the lysate was

cleared afterwards by centrifugation. As input samples, 5 µl of the expressions were mixed with 95 µl 2x SDS-PAGE sample buffer and boiled. Beads were washed three times with DNA pulldown buffer to remove unbound DNA and incubate with 20 µl *in-vitro* translated p63 in DNA pulldown buffer with a final volume of 400 µl for 3 h at 4 °C rotating. Afterwards beads were washed 4 times with 400 µl DNA pulldown buffer and bound proteins were eluted by incubation of the beads in 100 µl 1x LDS buffer supplemented with reducing agent for 10 min at 70°C. Input and pulldown samples were analysed by western blotting and quantified. For the relative pull-down efficiency each pulldown sample was normalized to the input sample. The DNA pull-down assays were performed as three independent biological replicates. Statistical significance was assessed by ordinary one-way ANOVA followed by Tukey's post hoc test using Graphpad Prism 8.

Solubility assay

To further investigate the aggregation state of the p53 mutants and isoforms within the cells, a solubility assay was performed. Cells were transfected one day after seeding in 12-well plates. 24 hours after transfection, cells were washed with 1 mL PBS, harvested with accutase and spun down. The supernatant was aspirated, and the cell pellet was washed again with PBS followed by centrifugation. Afterwards, the cells were lysed with 100 µL solubility buffer A (20 mM Tris (pH 7.5), 150 mM NaCl, 1 mM DTT, 2 mM $MgCl_2$, 1% Triton X-100) with 1 µL benzonase for 60 min on ice. Followed by centrifuging for 15 min at 13000 rpm at 4 °C. 75 µL of the supernatant (containing the soluble fraction) was mixed with 25 µL 5x SDS sample buffer. Remaining supernatant was discharged and the pellet (containing the insoluble fraction) was resuspended in 100 µL in solubility buffer B (20 mM Tris (pH 7.5), 150 mM NaCl, 1 mM DTT, 2 mM $MgCl_2$, 1% SDS). The samples were incubated for 20 min at room temperature. After incubation, the samples were spun down for 15 min at 13000 rpm at room temperature. 75 µL of the supernatant were mixed with 25 µL 5x SDS sample buffer. The samples were incubated at 95 °C for 10 min. Protein levels were analyzed by Western blot. The solubility assays were performed as three independent biological replicates. Statistical significance was assessed by ordinary one-way ANOVA followed by Tukey's post hoc test using Graphpad Prism 8. To investigate the effect of chaperones on the solubility of p53 isoforms cells were transfected and treated with different inhibitors one day after seeding in 12-well plates. 24 hours after transfection the solubility assay was performed as described above. The used inhibitors were JG-98 (HSP70 inhibitor, final concentration 5 µM, MedChem Express), YM-1 (HSP70 inhibitor, final concentration 10 µM, MedChem Express), VER-155008 (HSP70 inhibitor, final concentration 10 µM, MedChem Express) and 17-AAG (HSP90 inhibitor, final concentration 2 µM, MedChem Express).

Reticulocyte lysate protein expression

Proteins were translated *in-vitro* using the TnT Coupled Reticulocyte Lysate System (Promega). Constructs in a pcDNA3.1(+) vector were diluted to 100 ng/µl and mixed in a 1:4 volume ratio with rabbit reticulocyte lysate (RRL) and incubated for 90 min at 30 °C. The reaction was stopped by adding Benzonase (Millipore) for 30 min at 4 °C. The supernatant was cleared by centrifugation at 16,100 × *g* for 10 min at 4 °C and stored on ice until use.

DARPin Pulldown assays

Target proteins were *in-vitro* translated. An excess of biotinylated DARPins was pre-incubated with pre-equilibrated magnetic Pierce™ Streptavidin Beads (Thermo Fisher Scientific) in Pulldown (PD) wash buffer (50 mM HEPES, pH 7.5, 200 mM NaCl, 0.1 % (v/v) Tween-20, 0.5mM TCEP) while rotating for 1 h at 4 °C. The magnetic beads were washed three times with PD wash buffer to remove unbound DARPins and were resuspended in PD wash buffer with the same volume as before to maintain magnetic bead concentrations. 10 µl DARPin loaded beads were mixed with 10 µl *in-vitro* translated protein and adjusted to a total volume of 400 µl with PD wash buffer. The PD mix was incubated while rotating 3 h at 4 °C. Pulldown samples were washed five times with 400 µl PD wash buffer and eluted with 1x LDS buffer (Thermo Fisher Scientific, supplemented with reducing agent) by boiling at 70 °C for 10 min. Samples were analyzed by Western blot. The DARPin pull-down assays were performed as three independent biological replicates. Statistical significance was assessed by ordinary one-way ANOVA followed by Tukey's post hoc test using Graphpad Prism 8.

HPV E6 degradation assay

The E6 protein from HPV is able to induce p53 hyper-degradation, consequently inactivate p53 when the DBD of p53 is correctly folded (65). N-terminally Myc-tagged proteins were *in-vitro* translated using RRL. Lysates were diluted in reaction buffer (25 mM HEPES ph 7.5, 150 mM NaCl, 0.5 mM TCEP, 1 mM $MgCl_2$, 1 mM ATP) and supplemented with either 5 µM GST-tagged HPV16 E6 or GST only as control. Reactions were incubated for 4 h at 25°C. The reaction was stopped with addition of 30 µL 2x SDS sample buffer and incubation for 3 min at 95 °C. Protein levels were analyzed by Western blot. The HPV E6 assays were performed as three independent biological replicates. Statistical significance was assessed by ordinary one-way ANOVA followed by Tukey's post hoc test using Graphpad Prism 8.

Co-Immunoprecipitation

For Co-immunoprecipitation (co-IP), H1299 cells were co-transfected with either HA-tagged wtp53, p63 or p73 and different isoforms of Myc-tagged p53. For Co-IP with endogenous HSC/HSP70, H1299 cells were transfected with Myc-tagged p53 variants alone. Twenty-four

hours after transfection, cells were collected and lysed on ice in RIPA lysis buffer (50 mM HEPES (pH 7.5), 150 mM NaCl, 1% Nonidet P-40, 1% sodium deoxycholate, 2 mM $MgCl_2$,1 mM DTT) with the addition of protease and phosphatase inhibitors. Lysates were cleared by centrifugation and incubated with 0.5 µg of HA-antibody or HSC/HSP70-antibody overnight at 4 °C. The immunocomplexes were removed from the lysate using 12 µL Protein G Dynabeads (Thermo Fisher Scientific), washed four times with ice-cold IP wash buffer (50 mM Tris (pH 7.8), 150 mM NaCl, 0.1% Tween-20) and eluted with 1x LDS-sample buffer (Thermo Fisher Scientific) supplemented with reducing agent (Thermo Fisher Scientific) for 10 min at 70 °C. Samples were analysed by Western blotting. Relative immunoprecipitation efficiency was calculated by normalisation of the IP western blot signal to the respective input signal.

Conformation-specific Immunoprecipitation

For Conformation-specific Immunoprecipitation (Conf-IP), H1299 cells were transfected with empty vector or N-terminally Myc-tagged p53 variants. p53 isoforms were immunoprecipitated (IP) with either α-Myc or α-p53 antibody (pAB240). The latter binds an epitope in the DBD of p53, which is only exposed when the domain is unfolded (66). Twenty-four hours after transfection, cells were collected and lysed on ice in RIPA lysis buffer (50 mM HEPES (pH 7.5), 150 mM NaCl, 1% Nonidet P-40, 1% sodium deoxycholate, 2 mM $MgCl_2$,1 mM DTT) with the addition of protease and phosphatase inhibitors. Lysates were cleared by centrifugation and incubated with 0.5 µg of α-Myc or pAB240 antibody overnight at 4 °C. The immunocomplexes were removed from the lysate using 12 µL Protein G Dynabeads (Thermo Fisher Scientific), washed four times with ice-cold IP wash buffer (50 mM Tris (pH 7.8), 150 mM NaCl, 0.1% Tween-20) and eluted with 1x LDS-sample buffer (Thermo Fisher Scientific) supplemented with reducing agent (Thermo Fisher Scientific) for 10 min at 70 °C. Samples were analysed by Western blotting. Relative immunoprecipitation efficiency was calculated by normalisation of the IP western blot signal to the respective input signal.

Statistical Analysis

If not stated otherwise, experiments were performed as three independent biological replicates followed by statistical analysis (standard deviation SD; n=3) and statistical significance was assessed by ordinary one-way ANOVA (n.s.: $P > 0.05$, *: $P \leq 0.05$, **: $P \leq 0.01$, ***: $P \leq 0.001$, ****: $P \leq 0.0001$) followed by Tukey's post hoc test using Graphpad Prism 8.

Data availability

The mass spectrometry proteomics data have been deposited to the ProteomeXchange Consortium via the PRIDE (67) partner repository with the dataset identifier PXD045655. The

data from the second, p53 peptide specific mass spectrometry experiment have been deposited with the dataset identifier PXD058245. Analysis scripts are available upon request.

Acknowledgements

We thank Marina Hoffmann for help with deposition of the mass spectrometry data to the PRIDE server. Funding was provided by the Deutsche Krebshilfe (Grant number 70113956), the Centre for Biomolecular Magnetic Resonance (BMRZ) and the Clusterproject ENABLE (funded by the Hessian Ministry for Science and the Arts).

References

1. Joerger, A.C., Ang, H.C. and Fersht, A.R. (2006) Structural basis for understanding oncogenic p53 mutations and designing rescue drugs. *Proc Natl Acad Sci U S A*, **103**, 15056-15061.
2. Funk, J.S., Klimovich, M., Drangenstein, D., Pielhoop, O., Hunold, P., Borowek, A., Noeparast, M., Pavlakis, E., Neumann, M., Balourdas, D.I. *et al.* (2025) Deep CRISPR mutagenesis characterizes the functional diversity of TP53 mutations. *Nat Genet*, **57**, 140-153.
3. Haupt, Y., Maya, R., Kazaz, A. and Oren, M. (1997) Mdm2 promotes the rapid degradation of p53. *Nature*, **387**, 296-299.
4. Kubbutat, M.H., Jones, S.N. and Vousden, K.H. (1997) Regulation of p53 stability by Mdm2. *Nature*, **387**, 299-303.
5. Joerger, A.C. and Fersht, A.R. (2007) Structural biology of the tumor suppressor p53 and cancer-associated mutants. *Adv Cancer Res*, **97**, 1-+.
6. Osterburg, C., Ferniani, M., Antonini, D., Frombach, A.S., D'Auria, L., Osterburg, S., Lotz, R., Lohr, F., Kehrloesser, S., Zhou, H. *et al.* (2023) Disease-related p63 DBD mutations impair DNA binding by distinct mechanisms and varying degree. *Cell Death Dis*, **14**, 274.
7. Celli, J., Duijf, P., Hamel, B.C., Bamshad, M., Kramer, B., Smits, A.P., Newbury-Ecob, R., Hennekam, R.C., Van Buggenhout, G., van Haeringen, A. *et al.* (1999) Heterozygous germline mutations in the p53 homolog p63 are the cause of EEC syndrome. *Cell*, **99**, 143-153.
8. Osterburg, C. and Dotsch, V. (2022) Structural diversity of p63 and p73 isoforms. *Cell Death Differ*, **29**, 921-937.
9. Bourdon, J.C., Fernandes, K., Murray-Zmijewski, F., Liu, G., Diot, A., Xirodimas, D.P., Saville, M.K. and Lane, D.P. (2005) p53 isoforms can regulate p53 transcriptional activity. *Genes Dev*, **19**, 2122-2137.
10. Graupner, V., Schulze-Osthoff, K., Essmann, F. and Janicke, R.U. (2009) Functional characterization of p53beta and p53gamma, two isoforms of the tumor suppressor p53. *Cell Cycle*, **8**, 1238-1248.
11. Bullock, A.N., Henckel, J., DeDecker, B.S., Johnson, C.M., Nikolova, P.V., Proctor, M.R., Lane, D.P. and Fersht, A.R. (1997) Thermodynamic stability of wild-type and mutant p53 core domain. *Proc Natl Acad Sci U S A*, **94**, 14338-14342.
12. Xu, J., Reumers, J., Couceiro, J.R., De Smet, F., Gallardo, R., Rudyak, S., Cornelis, A., Rozenski, J., Zwolinska, A., Marine, J.C. *et al.* (2011) Gain of function of mutant p53 by coaggregation with multiple tumor suppressors. *Nat Chem Biol*, **7**, 285-295.

13. Levine, A.J., Wu, M.C., Chang, A., Silver, A., Attiyeh, E.F., Lin, J. and Epstein, C.B. (1995) The spectrum of mutations at the p53 locus. Evidence for tissue-specific mutagenesis, selection of mutant alleles, and a "gain of function" phenotype. *Ann N Y Acad Sci*, **768**, 111-128.
14. Zhang, Y.X., Pan, W.Y. and Chen, J. (2019) p53 and its isoforms in DNA double-stranded break repair. *J Zhejiang Univ Sci B*, **20**, 457-466.
15. Horikawa, I., Fujita, K., Jenkins, L.M., Hiyoshi, Y., Mondal, A.M., Vojtesek, B., Lane, D.P., Appella, E. and Harris, C.C. (2014) Autophagic degradation of the inhibitory p53 isoform Delta133p53alpha as a regulatory mechanism for p53-mediated senescence. *Nat Commun*, **5**, 4706.
16. Gadea, G., Arsic, N., Fernandes, K., Diot, A., Joruiz, S.M., Abdallah, S., Meuray, V., Vinot, S., Anguille, C., Remenyi, J. *et al.* (2016) TP53 drives invasion through expression of its Delta133p53beta variant. *Elife*, **5**.
17. Roth, I., Campbell, H., Rubio, C., Vennin, C., Wilson, M., Wiles, A., Williams, G., Woolley, A., Timpson, P., Berridge, M.V. *et al.* (2016) The Delta133p53 isoform and its mouse analogue Delta122p53 promote invasion and metastasis involving pro-inflammatory molecules interleukin-6 and CCL2. *Oncogene*, **35**, 4981-4989.
18. Fujita, K., Mondal, A.M., Horikawa, I., Nguyen, G.H., Kumamoto, K., Sohn, J.J., Bowman, E.D., Mathe, E.A., Schetter, A.J., Pine, S.R. *et al.* (2009) p53 isoforms Delta133p53 and p53beta are endogenous regulators of replicative cellular senescence. *Nat Cell Biol*, **11**, 1135-1142.
19. Mondal, A.M., Horikawa, I., Pine, S.R., Fujita, K., Morgan, K.M., Vera, E., Mazur, S.J., Appella, E., Vojtesek, B., Blasco, M.A. *et al.* (2013) p53 isoforms regulate aging- and tumor-associated replicative senescence in T lymphocytes. *J Clin Invest*, **123**, 5247-5257.
20. Turnquist, C., Horikawa, I., Foran, E., Major, E.O., Vojtesek, B., Lane, D.P., Lu, X., Harris, B.T. and Harris, C.C. (2016) p53 isoforms regulate astrocyte-mediated neuroprotection and neurodegeneration. *Cell Death Differ*, **23**, 1515-1528.
21. von Muhlinen, N., Horikawa, I., Alam, F., Isogaya, K., Lissa, D., Vojtesek, B., Lane, D.P. and Harris, C.C. (2018) p53 isoforms regulate premature aging in human cells. *Oncogene*, **37**, 2379-2393.
22. Gong, L., Gong, H., Pan, X., Chang, C., Ou, Z., Ye, S., Yin, L., Yang, L., Tao, T., Zhang, Z. *et al.* (2015) p53 isoform Delta113p53/Delta133p53 promotes DNA double-strand break repair to protect cell from death and senescence in response to DNA damage. *Cell Res*, **25**, 351-369.
23. Joruiz, S.M. and Bourdon, J.C. (2016) p53 Isoforms: Key Regulators of the Cell Fate Decision. *Cold Spring Harbor perspectives in medicine*, **6**.
24. Krois, A.S., Ferreon, J.C., Martinez-Yamout, M.A., Dyson, H.J. and Wright, P.E. (2016) Recognition of the disordered p53 transactivation domain by the transcriptional adapter zinc finger domains of CREB-binding protein. *Proc Natl Acad Sci U S A*, **113**, E1853-1862.
25. Rohaly, G., Chemnitz, J., Dehde, S., Nunez, A.M., Heukeshoven, J., Deppert, W. and Dornreiter, I. (2005) A novel human p53 isoform is an essential element of the ATR-intra-S phase checkpoint. *Cell*, **122**, 21-32.
26. Senturk, S., Yao, Z., Camiolo, M., Stiles, B., Rathod, T., Walsh, A.M., Nemajerova, A., Lazzara, M.J., Altorki, N.K., Krainer, A. *et al.* (2014) p53Psi is a transcriptionally inactive p53 isoform able to reprogram cells toward a metastatic-like state. *Proc Natl Acad Sci U S A*, **111**, E3287-3296.
27. Chan, W.M. and Poon, R.Y. (2007) The p53 Isoform Deltap53 lacks intrinsic transcriptional activity and reveals the critical role of nuclear import in dominant-negative activity. *Cancer Res*, **67**, 1959-1969.
28. Martinez-Zapien, D., Ruiz, F.X., Poirson, J., Mitschler, A., Ramirez, J., Forster, A., Cousido-Siah, A., Masson, M., Vande Pol, S., Podjarny, A. *et al.* (2016) Structure of the E6/E6AP/p53 complex required for HPV-mediated degradation of p53. *Nature*, **529**, 541-545.
29. Wang, J.C.K., Baddock, H.T., Mafi, A., Foe, I.T., Bratkowski, M., Lin, T.Y., Jensvold, Z.D., López, M.P., Stokoe, D., Eaton, D. *et al.* (2024) Structure of the p53 degradation complex from HPV16. *Nature Communications*, **15**.

30. Munick, P., Strubel, A., Balourdas, D.I., Funk, J.S., Mernberger, M., Osterburg, C., Dreier, B., Schaefer, J.V., Tuppi, M., Yuksel, B. *et al.* (2025) DARPin-induced reactivation of p53 in HPV-positive cells. *Nat Struct Mol Biol*.
31. Strubel, A., Munick, P., Chaikuad, A., Dreier, B., Schaefer, J., Gebel, J., Osterburg, C., Tuppi, M., Schafer, B., Knapp, S. *et al.* (2022) Designed Ankyrin Repeat Proteins as a tool box for analyzing p63. *Cell Death Differ*, **29**, 2445-2458.
32. Wang, G. and Fersht, A.R. (2015) Propagation of aggregated p53: Cross-reaction and coaggregation vs. seeding. *Proc Natl Acad Sci U S A*, **112**, 2443-2448.
33. Russo, C., Osterburg, C., Sirico, A., Antonini, D., Ambrosio, R., Wurz, J.M., Rinnenthal, J., Ferniani, M., Kehrloesser, S., Schafer, B. *et al.* (2018) Protein aggregation of the p63 transcription factor underlies severe skin fragility in AEC syndrome. *Proc Natl Acad Sci U S A*, **115**, E906-E915.
34. McGrath, J.A., Duijf, P.H., Doetsch, V., Irvine, A.D., de Waal, R., Vanmolkot, K.R., Wessagowit, V., Kelly, A., Atherton, D.J., Griffiths, W.A. *et al.* (2001) Hay-Wells syndrome is caused by heterozygous missense mutations in the SAM domain of p63. *Hum Mol Genet*, **10**, 221-229.
35. Fernandez-Escamilla, A.M., Rousseau, F., Schymkowitz, J. and Serrano, L. (2004) Prediction of sequence-dependent and mutational effects on the aggregation of peptides and proteins. *Nat Biotechnol*, **22**, 1302-1306.
36. Cino, E.A., Soares, I.N., Pedrote, M.M., de Oliveira, G.A.P. and Silva, J.L. (2016) Aggregation tendencies in the p53 family are modulated by backbone hydrogen bonds. *Sci Rep-Uk*, **6**.
37. Brown, A.J., Gibson, S.J., Hatton, D. and James, D.C. (2017) In silico design of context-responsive mammalian promoters with user-defined functionality. *Nucleic acids research*, **45**, 10906-10919.
38. Gadella, T.W.J., van Weeren, L., Stouthamer, J., Hink, M.A., Wolters, A.H.G., Giepmans, B.G., Aumonier, S., Dupuy, J. and Royant, A. (2023) mScarlet3: a brilliant and fast-maturing red fluorescent protein. *Nature Methods*.
39. Beerten, J., Van Durme, J., Gallardo, R., Capriotti, E., Serpell, L., Rousseau, F. and Schymkowitz, J. (2015) WALTZ-DB: a benchmark database of amyloidogenic hexapeptides. *Bioinformatics*, **31**, 1698-1700.
40. Agoff, S.N., Hou, J., Linzer, D.I.H. and Wu, B. (1993) Regulation of the Human Hsp70 Promoter by P53. *Science*, **259**, 84-87.
41. Garcia-Alai, M.M., Tidow, H., Natan, E., Townsley, F.M., Veprintsev, D.B. and Fersht, A.R. (2008) The novel p53 isoform "delta p53" is a misfolded protein and does not bind the p21 promoter site. *Protein Sci*, **17**, 1671-1678.
42. Coutandin, D., Lohr, F., Niesen, F.H., Ikeya, T., Weber, T.A., Schafer, B., Zielonka, E.M., Bullock, A.N., Yang, A., Guntert, P. *et al.* (2009) Conformational stability and activity of p73 require a second helix in the tetramerization domain. *Cell Death Differ*, **16**, 1582-1589.
43. Joerger, A.C., Rajagopalan, S., Natan, E., Veprintsev, D.B., Robinson, C.V. and Fersht, A.R. (2009) Structural evolution of p53, p63, and p73: implication for heterotetramer formation. *Proc Natl Acad Sci U S A*, **106**, 17705-17710.
44. Gebel, J., Luh, L.M., Coutandin, D., Osterburg, C., Lohr, F., Schafer, B., Frombach, A.S., Sumyk, M., Buchner, L., Krojer, T. *et al.* (2016) Mechanism of TAp73 inhibition by DeltaNp63 and structural basis of p63/p73 hetero-tetramerization. *Cell Death Differ*, **23**, 1930-1940.
45. Kehrloesser, S., Osterburg, C., Tuppi, M., Schafer, B., Vousden, K.H. and Dotsch, V. (2016) Intrinsic aggregation propensity of the p63 and p73 TI domains correlates with p53R175H interaction and suggests further significance of aggregation events in the p53 family. *Cell Death Differ*, **23**, 1952-1960.
46. Deutsch, G.B., Zielonka, E.M., Coutandin, D., Weber, T.A., Schafer, B., Hannewald, J., Luh, L.M., Durst, F.G., Ibrahim, M., Hoffmann, J. *et al.* (2011) DNA damage in oocytes induces a switch of the quality control factor TAp63alpha from dimer to tetramer. *Cell*, **144**, 566-576.

47. Yang, A., Kaghad, M., Wang, Y., Gillett, E., Fleming, M.D., Dotsch, V., Andrews, N.C., Caput, D. and McKeon, F. (1998) p63, a p53 homolog at 3q27-29, encodes multiple products with transactivating, death-inducing, and dominant-negative activities. *Mol Cell*, **2**, 305-316.
48. Luh, L.M., Kehrloesser, S., Deutsch, G.B., Gebel, J., Coutandin, D., Schafer, B., Agostini, M., Melino, G. and Dotsch, V. (2013) Analysis of the oligomeric state and transactivation potential of TAp73alpha. *Cell Death Differ*, **20**, 1008-1016.
49. Levine, A.J. (2020) p53: 800 million years of evolution and 40 years of discovery. *Nat Rev Cancer*, **20**, 471-480.
50. Kouwenhoven, E.N., Oti, M., Niehues, H., van Heeringen, S.J., Schalkwijk, J., Stunnenberg, H.G., van Bokhoven, H. and Zhou, H. (2015) Transcription factor p63 bookmarks and regulates dynamic enhancers during epidermal differentiation. *EMBO Rep*, **16**, 863-878.
51. Suh, E.K., Yang, A., Kettenbach, A., Bamberger, C., Michaelis, A.H., Zhu, Z., Elvin, J.A., Bronson, R.T., Crum, C.P. and McKeon, F. (2006) p63 protects the female germ line during meiotic arrest. *Nature*, **444**, 624-628.
52. Marshall, C.B., Mays, D.J., Beeler, J.S., Rosenbluth, J.M., Boyd, K.L., Santos Guasch, G.L., Shaver, T.M., Tang, L.J., Liu, Q., Shyr, Y. *et al.* (2016) p73 Is Required for Multiciliogenesis and Regulates the Foxj1-Associated Gene Network. *Cell Rep*, **14**, 2289-2300.
53. Logotheti, S., Pavlopoulou, A., Marquardt, S., Takan, I., Georgakilas, A.G. and Stiewe, T. (2022) p73 isoforms meet evolution of metastasis. *Cancer Metast Rev*, **41**, 853-869.
54. Dyson, H.J. and Wright, P.E. (2025) How does p53 work? Regulation by the intrinsically disordered domains. *Trends in Biochemical Sciences*, **50**, 9-17.
55. Vieler, M. and Sanyal, S. (2018) p53 Isoforms and Their Implications in Cancer. *Cancers*, **10**.
56. Lei, J., Qi, R., Tang, Y., Wang, W., Wei, G., Nussinov, R. and Ma, B. (2019) Conformational stability and dynamics of the cancer-associated isoform Delta133p53beta are modulated by p53 peptides and p53-specific DNA. *FASEB J*, **33**, 4225-4235.
57. Arsic, N., Slatter, T., Gadea, G., Villain, E., Fournet, A., Kazantseva, M., Allemand, F., Sibille, N., Seveno, M., de Rossi, S. *et al.* (2021) Delta 133p53 beta isoform pro-invasive activity is regulated through an aggregation-dependent mechanism in cancer cells. *Nature Communications*, **12**.
58. Chen, C., Gorlatova, N., Kelman, Z. and Herzberg, O. (2011) Structures of p63 DNA binding domain in complexes with half-site and with spacer-containing full response elements. *P Natl Acad Sci USA*, **108**, 6456-6461.
59. Timofeev, O., Koch, L., Niederau, C., Tscherne, A., Schneikert, J., Klimovich, M., Elmshauser, S., Zeitlinger, M., Mernberger, M., Nist, A. *et al.* (2020) Phosphorylation Control of p53 DNA-Binding Cooperativity Balances Tumorigenesis and Aging. *Cancer Research*, **80**, 5231-5244.
60. Liu, J., Lin, M.H., Zhang, C., Wang, D.D., Feng, Z.H. and Hu, W.W. (2012) TAp63 gamma enhances nucleotide excision repair through transcriptional regulation of DNA repair genes. *DNA Repair*, **11**, 167-176.
61. Tyanova, S., Temu, T. and Cox, J. (2016) The MaxQuant computational platform for mass spectrometry-based shotgun proteomics. *Nat Protoc*, **11**, 2301-2319.
62. Cox, J., Neuhauser, N., Michalski, A., Scheltema, R.A., Olsen, J.V. and Mann, M. (2011) Andromeda: a peptide search engine integrated into the MaxQuant environment. *J Proteome Res*, **10**, 1794-1805.
63. Elias, J.E. and Gygi, S.P. (2007) Target-decoy search strategy for increased confidence in large-scale protein identifications by mass spectrometry. *Nat Methods*, **4**, 207-214.
64. Straub, W.E., Weber, T.A., Schafer, B., Candi, E., Durst, F., Ou, H.D., Rajalingam, K., Melino, G. and Dotsch, V. (2010) The C-terminus of p63 contains multiple regulatory elements with different functions. *Cell Death Dis*, **1**, e5.
65. Scheffner, M., Werness, B.A., Huibregtse, J.M., Levine, A.J. and Howley, P.M. (1990) The E6 oncoprotein encoded by human papillomavirus types 16 and 18 promotes the degradation of p53. *Cell*, **63**, 1129-1136.

66. Schmieg, F.I. and Simmons, D.T. (1993) p53 mutants with changes in conserved region II: three classes with differing antibody reactivity, SV40 T antigen binding and ability to inhibit transformation of rat cells. *Oncogene*, **8**, 2043-2050.
67. Perez-Riverol, Y., Bai, J., Bandla, C., Garcia-Seisdedos, D., Hewapathirana, S., Kamatchinathan, S., Kundu, D.J., Prakash, A., Frericks-Zipper, A., Eisenacher, M. *et al.* (2022) The PRIDE database resources in 2022: a hub for mass spectrometry-based proteomics evidences. *Nucleic acids research*, **50**, D543-D552.

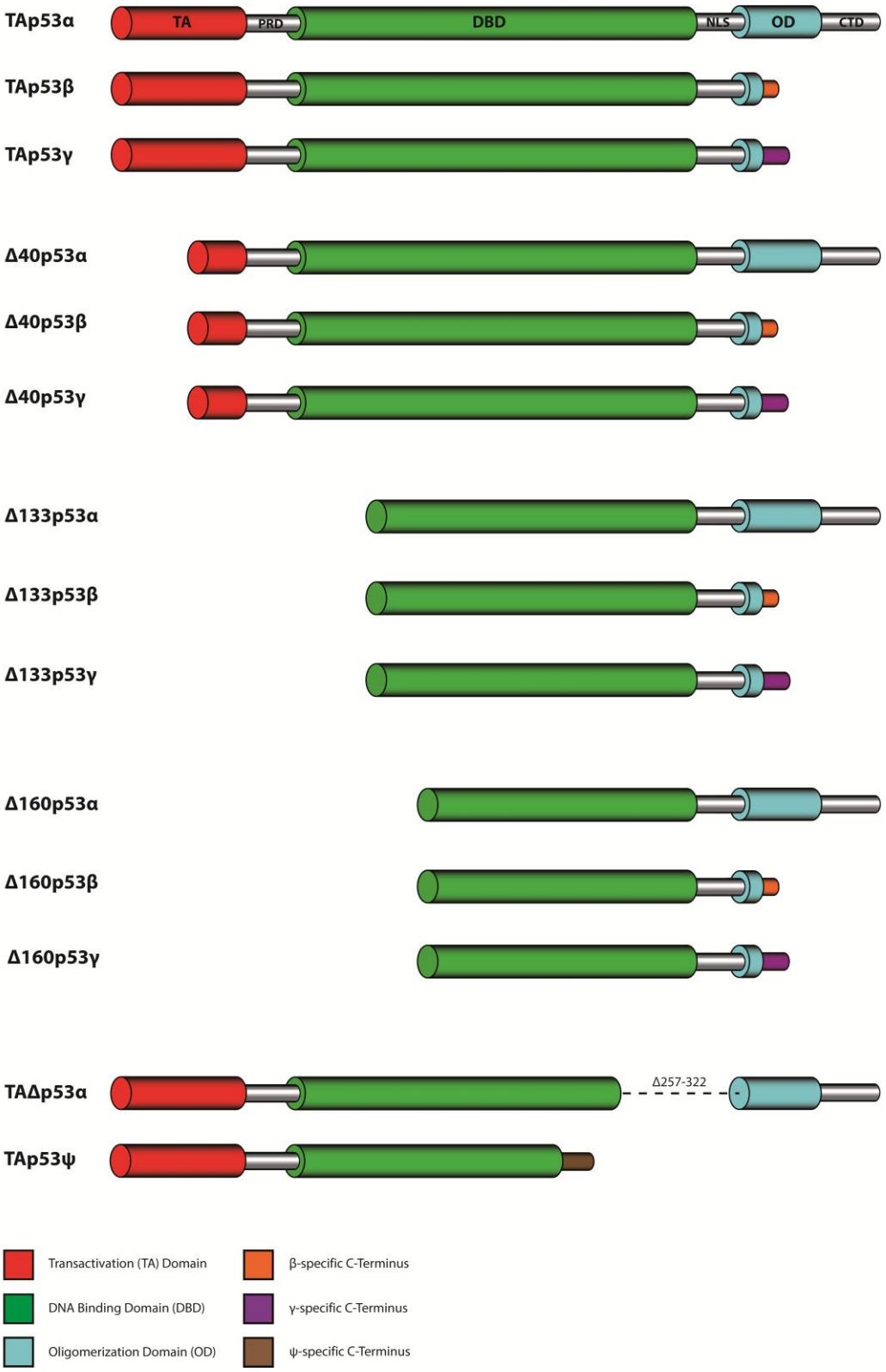

Figure 1 Domain organization of p53 isoforms. Overview of the so far described p53 isoforms that are formed by a combination of four N-terminal (TAp53, Δ40p53, Δ133p53 and Δ160p53) and three C-terminal variants (α, β and γ), leading to 12 individual p53 isoforms. The remaining two isoforms p53ψ (or TAp53ψ) and Δp53 (or TAΔp53α) are generated by alternative splicing.

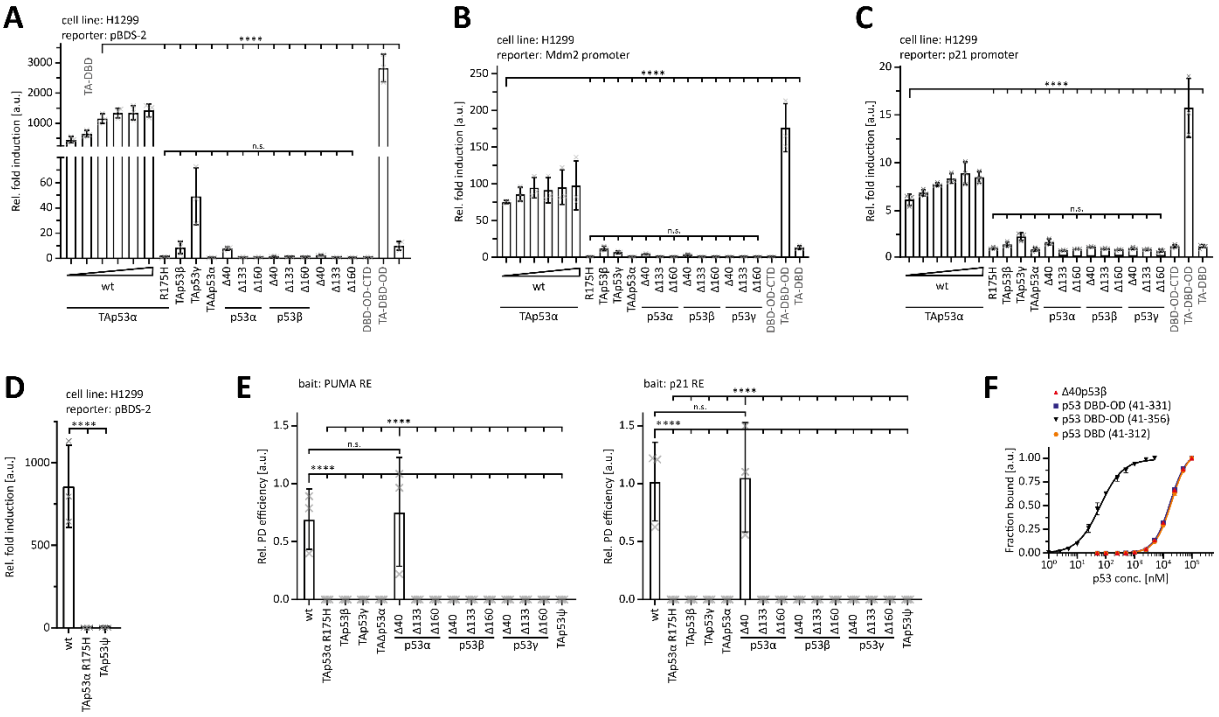

Figure 2 Activity, oligomerization and DNA binding. Luciferase reporter assay of p53 isoforms and variants either on the pBDS-2 reporter (three repeats of the 14-3-3σ promoter RE) **(A)**, or on the Mdm2 promoter **(B)**, or on the p21 promoter **(C)**. TAp53α carrying the cancer-related R175H mutation served as a negative control. H1299 cells **(A, B)** or Saos-2 cells **(C)** were transiently transfected with the respective luciferase reporter plasmids and the N-terminally Myc-tagged proteins. The plasmid encoding for TAp53α was titrated with the remaining DNA amount for transfection being filled up with empty vector. **(D)** Luciferase reporter assay of p53ψ on the pBDS-2 reporter. TAp53α carrying the cancer-related R175H mutation served as a negative control. H1299 cells were transiently transfected with the respective luciferase reporter plasmids and the N-terminally Myc-tagged proteins. **(E)** DNA pull-down assay of p53 isoforms with the 20bp REs of the human PUMA and p21 promoter as bait. TAp53α carrying the cancer-related R175H mutation served as a negative control. N-terminally Myc-tagged proteins were *in-vitro* translated using RRL. For the relative pull-down efficiency each pulldown signal was normalized to the input signal. **(F)** SPR affinity curves of purified Δ40p53β (red), p53 DBD-OD variants (purple and black) and the isolated p53 DBD (orange) binding to the 20bp p21 RE immobilized on a streptavidin (SA) chip. Data points were extracted by equilibrium analysis of sensograms as in (Supplementary Figure S1G), plotted and fitted with a non-linear, least squares regression using a single-exponential one-site binding model with Hill slope. p53 DBD-OD (41-356) encompasses the complete OD, while p53 DBD-OD (41-331) only has the N-terminal part of the OD common to all p53α, p53β and p53γ isoforms. (A-E) The bar diagram shows the mean values and error bars the corresponding SD (n=3). Statistical significance was assessed by ordinary one-way ANOVA (n.s.: P > 0.05, *: P ≤ 0.05, **: P ≤ 0.01, ***: P ≤ 0.001, ****: P ≤ 0.0001).

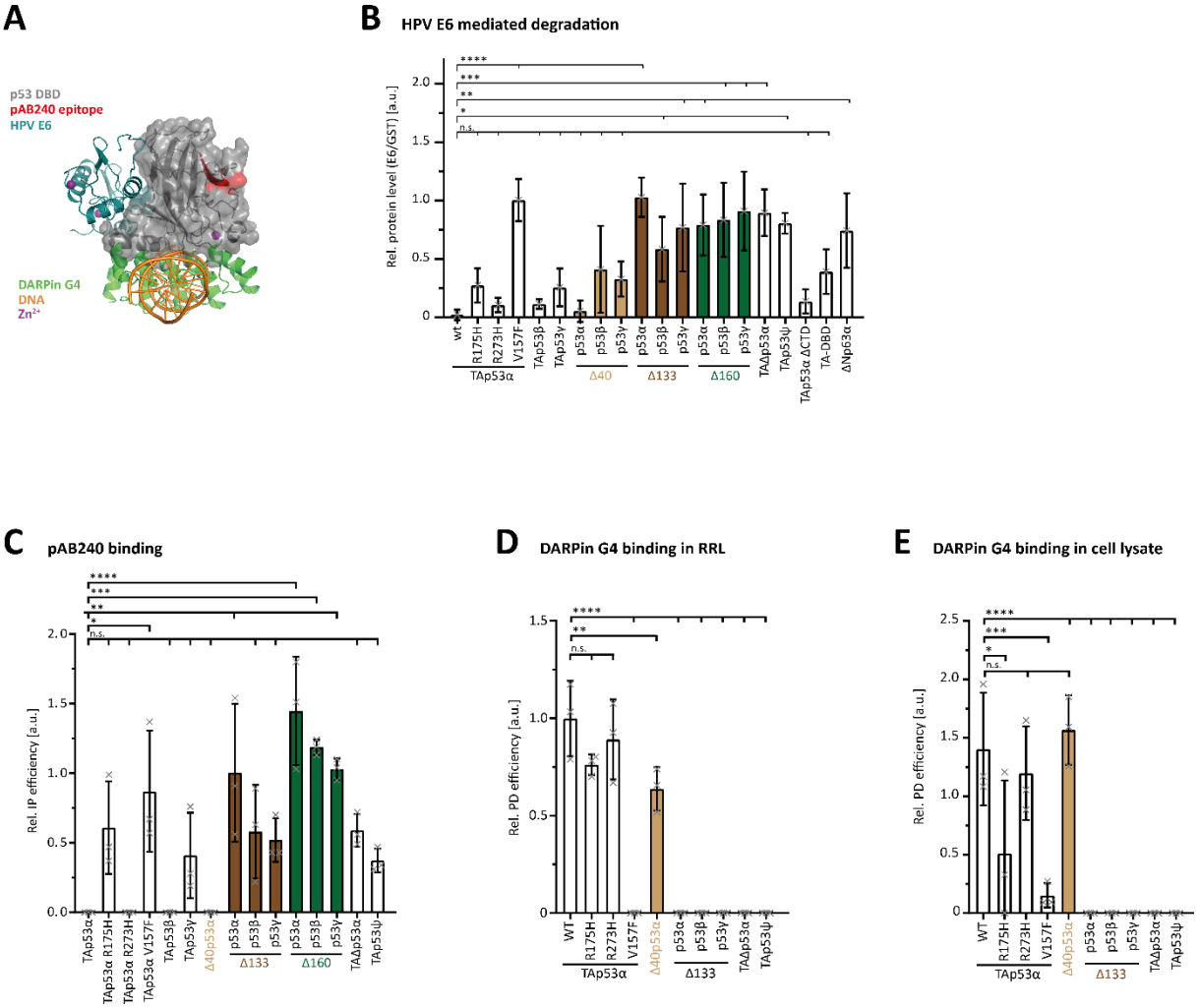

Figure 3 Probing the DBD Fold**. (A)** Superposition of structures of the p53 DBD (grey) in complex with DNA (orange; PDB: 3TS8), HPV16 E6 (blue; PDB: 4XR8) and DARPin G4 (green; PDB: 7Z7E). Epitope of the pAB240 is marked in red and the zinc ion is depicted as a purple sphere. **(B)** E6 degradation assay of p53 isoforms, cancer-related mutants, and variants. ΔNp63α served as a negative control. N-terminally Myc-tagged proteins were *in-vitro* translated using RRL. Lysates were diluted in reaction buffer and supplemented with either 5 µM GST-tagged HPV16 E6 or GST only as control. Reactions were incubated for 4 h at 25°C and analyzed for protein levels by WB. Signals were normalized to the loading control vinculin and the relative protein level ratio between E6 and GST samples were calculated by setting the normalized signal of the GST samples to 1. **(C)** Conformation-specific immunoprecipitation (Conf-IP) of p53 isoforms and cancer-related mutants. H1299 cells were transiently transfected with empty vector or N-terminally Myc-tagged p53 variants. p53 was immunoprecipitated (IP) with either α-mouse IgG or an α-p53 antibody (pAB240). The latter binds an epitope in the DBD of p53, which is only exposed when the domain is unfolded. Consequently, pAB240 only recognizes intrinsically unfolded p53 mutants under native IP conditions. Input and IP samples were subsequently analyzed by WB using α-Myc antibody. For the relative Conf-IP efficiency each IP signal was normalized to the input signal. **(D)** DARPin pull-down assay of p53 isoforms and cancer-related mutants *in-vitro* translated using RRL or transiently expressed in H1299 **(E)** with immobilized DARPin G4. DARPin G4 only recognizes the folded DBD of p53. For the relative pull-down efficiency each pulldown signal was normalized to the input signal. Note that the expression temperature in the RRL experiment was with 30°C lower than the temperature

in the cell culture experiment (37ºC) resulting in a higher level of folded R175H p53 mutant and hence a higher pulldown efficiency. (B,C,D,E) The bar diagram shows the mean values and error bars the corresponding SD (n=3). Statistical significance was assessed by ordinary one-way ANOVA (n.s.: $P > 0.05$, *: $P \leq 0.05$, **: $P \leq 0.01$, ***: $P \leq 0.001$, ****: $P \leq 0.0001$).

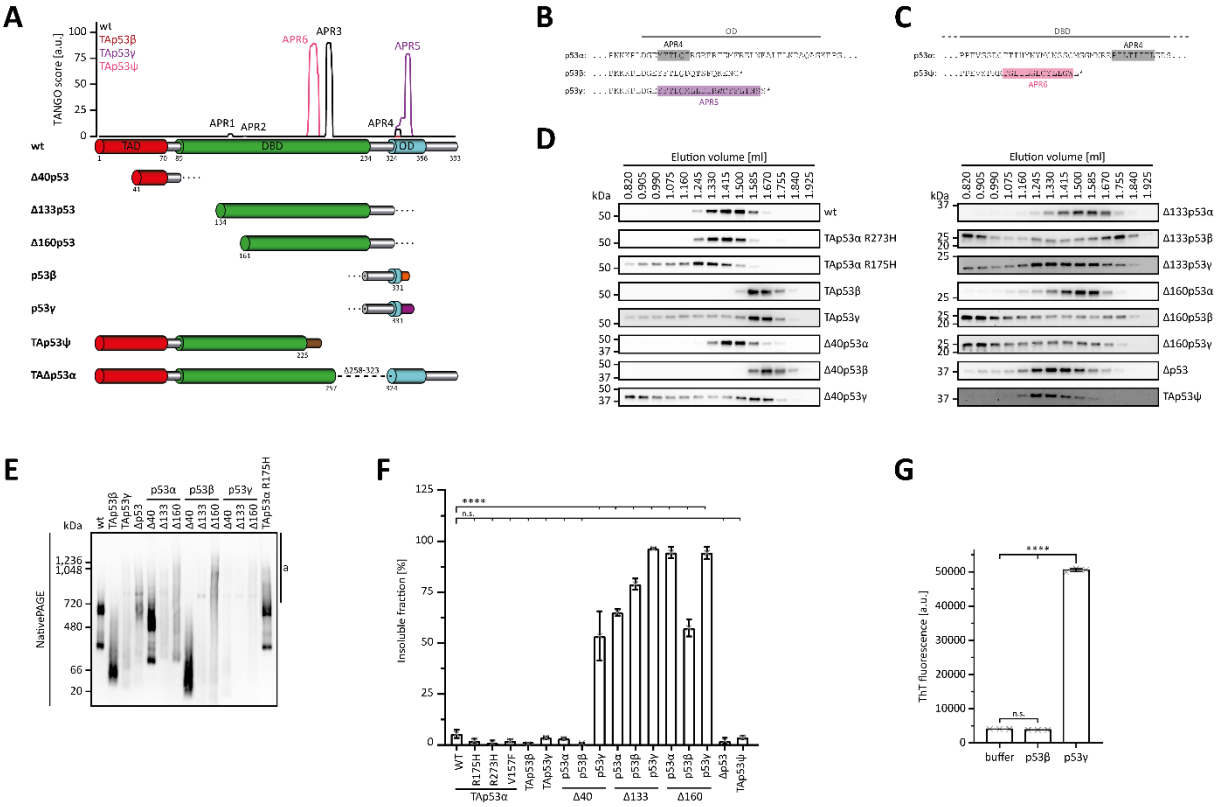

Figure 4 Aggregation and Solubility**. (A)** Predicted aggregation propensity of TAp53α (black) and the C-terminal isoforms TAp53β (auburn), TAp53γ (purple) and TAp53ψ (pink). TAp53α is predicted to have a total of four APRs (APR1-4) sharing the first three with TAp53β and TAp53γ. TAp53γ and TAp53ψ each introduced a novel APR (APR5 and APR6) with their specific C-termini. Schematic illustration of the boundaries of all N- and C-terminal p53 isoforms is shown below the graph. Position and length of the novel sequences introduced by the C-terminal are shown with the corresponding colours. All *in-silico* predictions were run using the TANGO algorithm with the following parameters: pH 7.5, 150 mM ionic strength and at a temperature of 37°C. **(B)** Sequence alignment of p53α with the p53β and p53γ specific C-termini. The boundaries of the OD are indicated by the grey line and the predicted APRs from (A) are highlighted in the respective colours. **(C)** Sequence alignment of p53α the p53 ψ specific C-terminus. The boundaries of the DBD are indicated by the grey line and the predicted APRs from (A) are highlighted in the respective colours. **(D)** Analytical SEC of p53 isoforms and cancer-related mutants. H1299 cells were transiently transfected with the N-terminally Myc-tagged proteins and cell lysates were loaded onto a Superose 6 SEC column. Both, lysis and running buffer contained 20 mM CHAPS. Collected fractions were analysed for p53 by WB using an α-Myc antibody. An elution volume of 0.820 ml corresponds to the void volume of the column (2.4 ml bed volume). **(E)** BN-PAGE of p53 isoforms and the cancer-related R175H mutant. H1299 cells were transiently transfected with the N-terminally Myc-tagged proteins. Cell lysates were subsequently analysed by BN-PAGE and SDS-PAGE (shown in figure supplement 3B) followed by WB using α-Myc antibody for detection. High molecular weight species corresponding to aggregates are marked by 'a'. **(F)** Solubility assay of p53 isoforms and cancer-related mutants. H1299 cells were transiently transfected with the indicated Myc-tagged proteins and lysed in a buffer supplemented with Triton X-100. Soluble and insoluble components were separated by centrifugation. The insoluble fraction in the pellet was solubilized with a buffer supplemented with SDS. Samples of both fractions were analysed by WB using α-Myc antibody. **(G)** Thioflavin T (ThT) fluorescence assay of the p53β (aa 322-341) and p53γ (322-346) C-termini. The peptides, solubilized in denaturation buffer, and denaturation buffer only as a control, were diluted 20-fold in assay buffer supplemented with

ThT and incubate at 37°C for 45 min. The final concentration of peptides and ThT was 20 µM and 25 µM, respectively. (F, G) The bar diagram shows the mean ThT fluorescence and error bars the corresponding SD (n=3). Statistical significance was assessed by ordinary one-way ANOVA (n.s.: $P > 0.05$, ****: $P \leq 0.0001$).

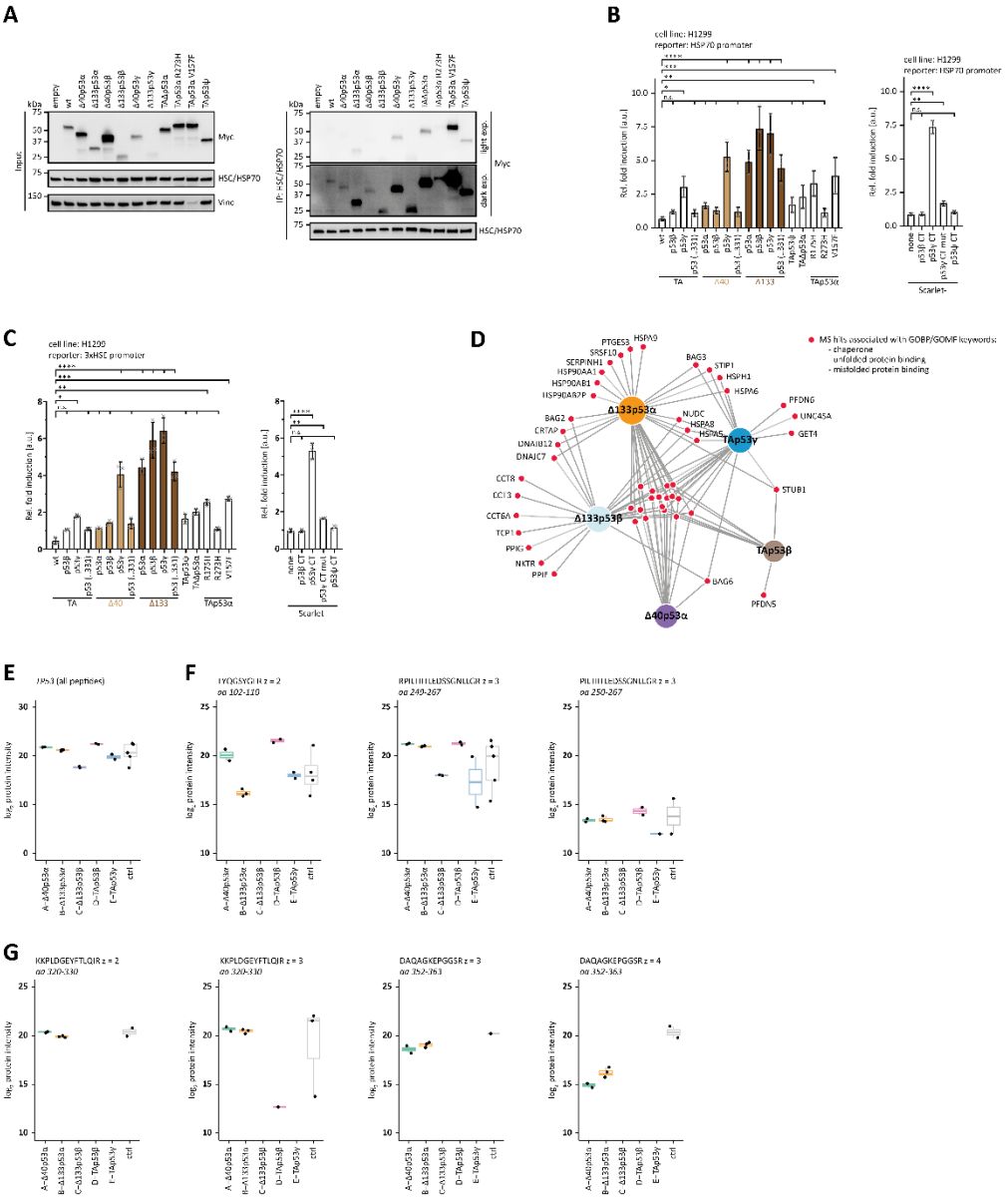

Figure 5 Chaperons. **(A)** Co-Immunoprecipitation of p53 isoforms and cancer-related mutants with endogenous HSC/HSP70. H1299 cells were transiently transfected with either empty vector or the indicated N-terminally Myc-tagged p53 variants. HSC/HSP70 was immunoprecipitated (IP) with an α-HSC/HSP70 antibody. Input and IP samples were subsequently analysed by WB using α-HSC/HSP70 and α-Myc antibody to detect HSC/HSP70 and p53 variants, respectively. A light and dark exposure of the IP samples detected with α-Myc antibody is shown. Vinculin served as a loading control for the input samples. **(B)** Luciferase reporter assay of p53 isoforms and mutants as well as the indicated Scarlet fusion proteins on the HSP70 promoter. H1299 cells were transiently transfected with the respective luciferase reporter plasmids and the N-terminally Myc-tagged proteins. **(B)** p53 (..331) contains only the C-terminal part common to p53α, p53β and p53γ. The fluorescent protein Scarlet was fused with the C-termini of p53 isoforms. Scarlet alone served as a negative control. **(C)** Luciferase reporter assay of p53 isoforms and mutants as well as the indicated Scarlet fusion proteins on the HSE promoter (containing three repeats of heat shock element). H1299 cells were transiently transfected with the respective luciferase reporter plasmids and the N-terminally Myc-tagged proteins. **(C)** p53 (..331) contains only the C-terminal part common to p53α, p53β and p53γ. The fluorescent protein Scarlet was fused with the C-termini of p53

isoforms. Scarlet alone served as a negative control. (B,C) The bar diagram shows the mean fold induction relative to the empty vector control and error bars the corresponding SD (n=3). Statistical significance was assessed by ordinary one-way ANOVA (n.s.: $P > 0.05$, *: $P \leq 0.05$, **: $P \leq 0.01$, ***: $P \leq 0.001$, ****: $P \leq 0.0001$). **(D)** Chaperons and other proteins associated with binding un-/misfolded proteins are shown, which are significantly enriched in the mass spectrometry analysis of p53 isoforms. The red nods represent the identified proteins assigned by the grey lines to the p53 isoforms they were enriched for. Significant hits were determined by setting the parameters: log2 enrichment greater than or equal to 0.5 and p-value less than 0.05 and proteins were filtered for the keywords ('chaperone', 'unfolded protein binding' and 'misfolded protein binding') in the GOBP (Gene Ontology Biological Process) and GOMF (Gene Ontology Molecular Function) terms. The plot was generated using DiVenn (v2.0). **(E)** Results from the second mass spectrometry experiment, focused on the quantification of p53 peptide precursors. As the biotin ligase was directly fused to p53, p53 peptides are quantified for all samples (log_2-transformed protein LFQ intensity). Negative controls represent data from unbiotinylated lysates (no biotin added). **(F)** Peptides from the DNA binding domains spanning residues 249-267 were quantified for all samples (log_2-scaled precursor intensity), consistent with this peptide being part of all investigated isoforms. A peptide spanning amino acids 102-110 was absent or beyond the detection limit in the Δ133p53β sample but quantified in all other samples. **(G)** Peptides originating from the oligomerization domain were reliably quantified in samples of isoforms containing a full length oligomerization domain (log_2-scaled precursor intensity), but not in samples of isoforms containing the β- and ɣ-C-termini (except for one low intense TAp53β precursor ion).

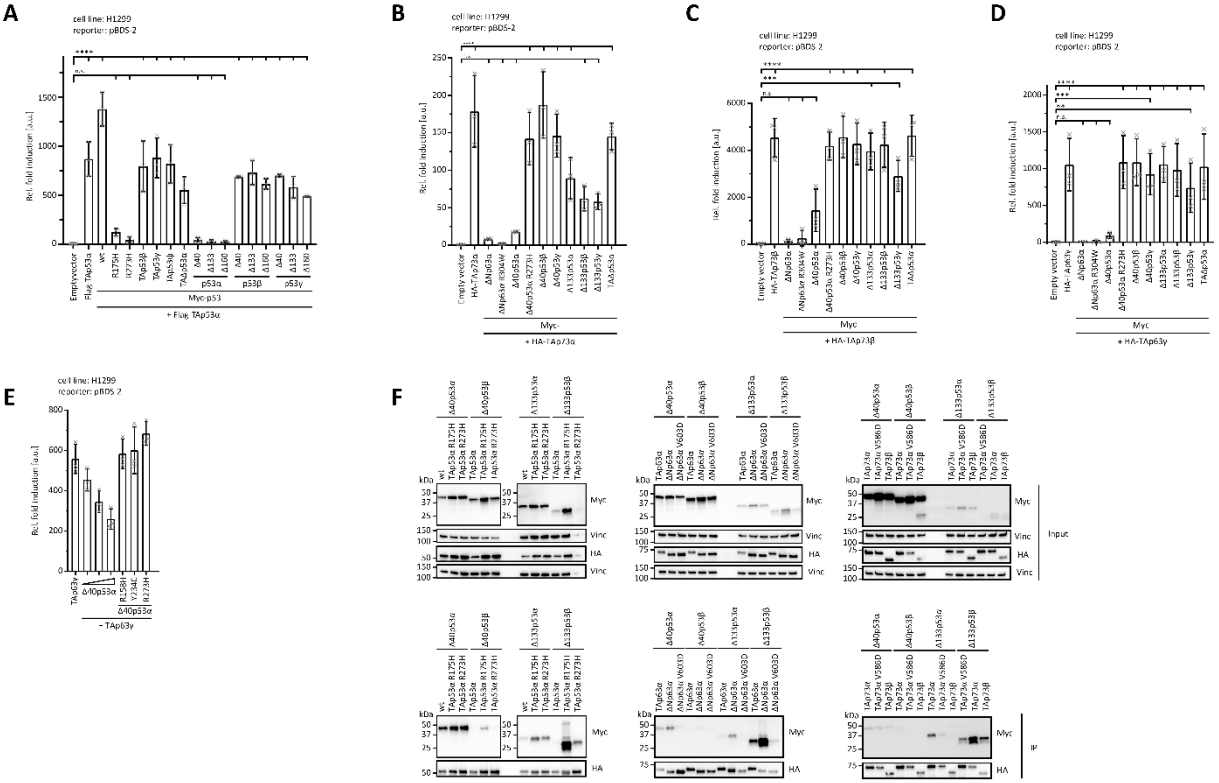

Figure 6 Inactivation of p53 family members. **(A)** Luciferase reporter assay of TAp53α in combination with p53 isoforms and cancer-related mutants on the pBDS-2 reporter. H1299 cells were transiently transfected with the respective luciferase reporter plasmids, the N-terminally Flag-tagged TAp53α alone or together with the N-terminally Myc-tagged p53 variants. Luciferase reporter assay of TAp73α **(B)**, TAp73β **(C)** or TAp63γ **(D)** in combination with p53 and p63 isoforms and cancer-related mutants on the pBDS-2 reporter. H1299 cells were transiently transfected with the respective luciferase reporter plasmids, the N-terminally HA-tagged TAp73α **(B)**, TAp73β **(C)** or TAp63γ **(D)** alone, empty vector or together with the N-terminally Myc-tagged p53/p63 variants. (A-D) The bar diagram shows the mean fold induction relative to the empty vector control and error bars the corresponding SD (n=3). Statistical significance was assessed by ordinary one-way ANOVA (n.s.: P > 0.05, *: P ≤ 0.05, **: P ≤ 0.01, ***: P ≤ 0.001, ****: P ≤ 0.0001). **(E)** Luciferase reporter assay of TAp63γ in combination with the Δ40p53α isoforms and cancer-related mutants on the pBDS-2 reporter. H1299 cells were transiently transfected with the respective luciferase reporter plasmids, the N-terminally Myc-tagged TAp63γ alone or together with the N-terminally Myc-tagged Δ40p53α variants. **(F)** Conformation-specific immunoprecipitation (Conf-IP) of p53, p63 or p73 isoforms and p53 variant (Δ40p53α, Δ40p53β, Δ133p53α and Δ133p53β). H1299 cells were transiently transfected with N-terminally HA-tagged p53, p63 or p73 isoforms and N-terminally Myc-tagged p53 variants (Δ40p53α, Δ40p53β, Δ133p53α and Δ133p53β). p53, p63, or p73 isoforms were immunoprecipitated (IP) with α-HA. p53α isoforms mostly hetero-tetramerize with different p53α isoforms, but co-aggregate with remaining p53 isoforms. p63 and p73 isoforms interact with p53 isoforms by co-aggregation. Input and IP samples were subsequently analysed by WB using α-Myc antibody.

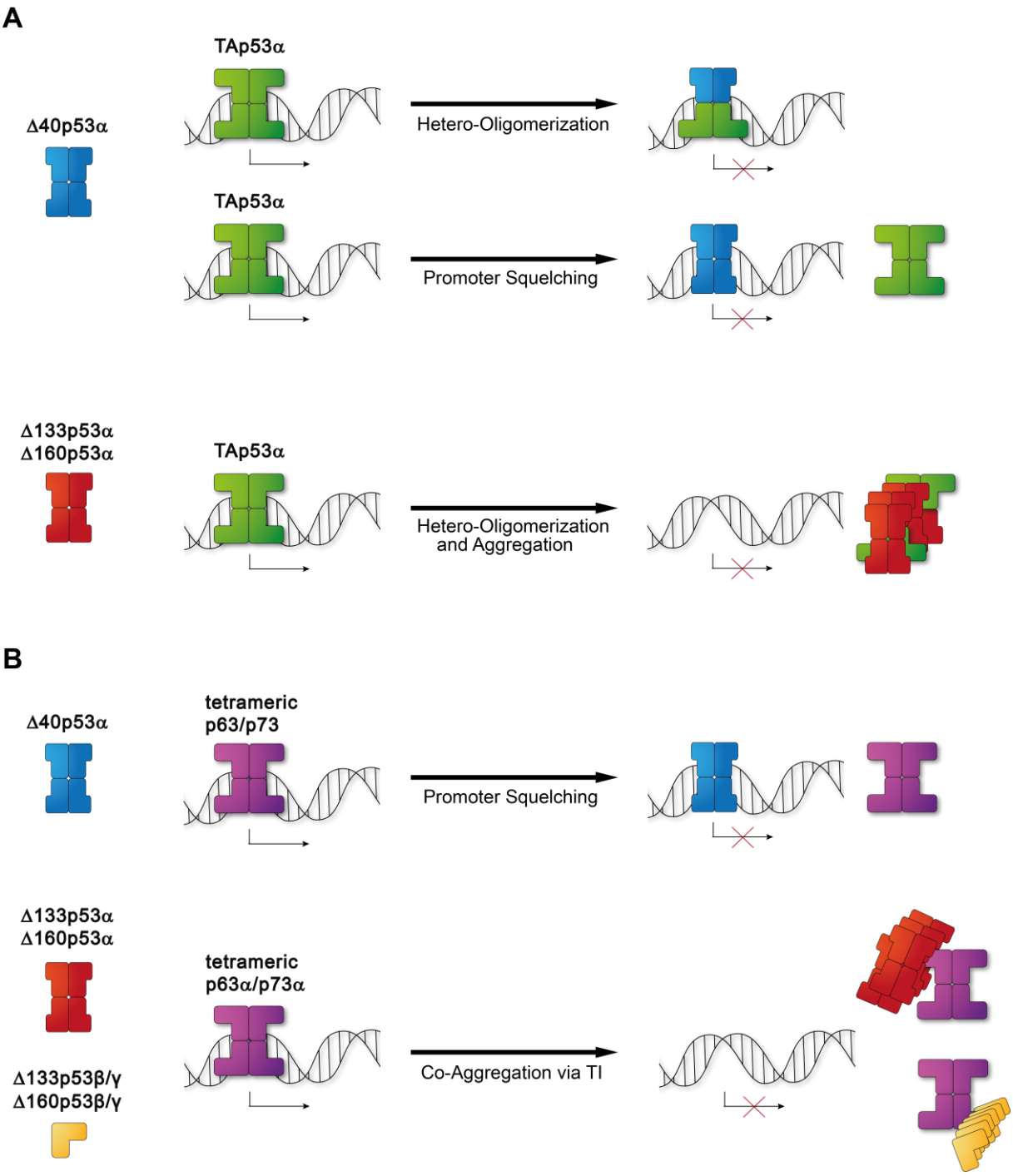

Figure 7 Mechanisms of inactivation within the p53 family. p53 isoforms have the potential to inactivate p53 family members via different mechanisms. **(A)** Either p53α isoforms form inactive hetero-tetramers (and/or aggregate) with wtp53 (Δ40p53α, Δ133p53α, Δ160p53α) and therefore inhibit wtp53 or inactive wtp53 by promotor squelching (Δ40p53α). **(B)** Furthermore, Δ40p53α isoform can as well inactivate tetrameric p63/p73 via promoter squelching. DBD-truncated aggregating p53 isoforms can co-aggregated with tetrameric p63α and p73α isoforms, but not with the closed TAp63α dimer.